Section II
Interstellar Matter

V.V. Sobolev and Physics of Gaseous Nebulae

A.F. Kholtygin[1], Yu.V. Milanova[1]

E-mail: *afkholtygin@gmail.com*

First works by V.V. Sobolev were devoted to gaseous nebulae. He proposed a method for determining the nebula temperature based on the analysis of the energy balance of the electron gas. He also investigated the transfer of L_α and L_c radiation and the role of light pressure in their dynamics. The works by V.V. Sobolev were at the bases of constructing the ionization models of gaseous nebulae. The Sobolev method is widely used in solving the problems of radiation transfer in the nebulae. In our report we review the impact of the ideas and methods proposed by V.V. Sobolev on both the classic and contemporary researches in physics of gaseous nebulae.

1 Introduction

There were about 200 papers published in 1800 − 1941 (according to ADS) before V.V. Sobolev started to study gaseous nebulae. First planetary nebulae, the Dumbbell Nebula M 27, was discovered by Ch. Messier in 1764 (see, e.g., [10]). W. Herschel proposed in 1791 that PNe derive their energy from a nearby star.

The first step towards an understanding of the nature of PNe was made by W. Huggins in 1864 with his spectroscopic observation of NGC 6543 [5]. He saw a single bright line in the spectra. Subsequent observations, with better resolution, showed that this bright line was actually the famous N_1+N_2 doublet.

Studying H_β, Menzel (1926) suggested that all the stellar outputs beyond the Lyman limit (912 Å) should be utilized to ionize the hydrogen atom [11]. In 1927 Zanstra supposed that H-lines are the result of the recombination of ionized hydrogen [20]. In 1928 Bowen identified the 8 strongest nebular lines as being due to metastable states of NII, OII and OIII [3].

In 1929 Perrine interpreted the broad (or even split) emission lines in PNe spectra as a result of an expansion of PNe [13] (not rotation as had been supposed before). In 1933 Ambartsumian found that the mean electron temperature of PNe is about of 10000 K [2].

For determination of the parameters of central stars (CS) of PNe, the methods by Zanstra [21] and Stoy [18] were proposed. In 1938 Whipple established that PNe ages are in the interval 10^3–10^5 years [19]. The physics of PNe was considered in the series of 18 papers written by Menzel and Aller in 1937–1945 (see [1]).

Here we review the papers by V.V. Sobolev which influenced on our understanding of the physics of planetary nebulae.

---

[1] Saint Petersburg State University, Russia

V. Grinin et al. (eds) Radiation mechanisms of astrophysical objects. Yerevan: Edit Print, 2017, pp. 99–104.

2 Sobolev's works on physics of gaseous nebulae

V.V. Sobolev started to study the PNe when he was still a graduate student by V.A. Ambartsumian.

Here we list the early papers by Sobolev which were not included in ADS:

1) *V. V. Sobolev,* "Determination of electron temperatures of planetary nebulae and improvement of the method of nebulium to determine the temperature of their central stars," Trudy Astron. Obs. Leningr. Univ., **12**, 3–16, 1941;
2) *V. V. Sobolev,* "Light pressure in the expanding nebula," Astron. Zh., **21**, 143–148, 1944;
3) *V.A. Ambartsumian, E.R. Mustel, A.B. Severnyi, V. V. Sobolev,* Teoreticheskaya Astrophysika. Moscow: GITTL, 1952;
4) *V. V. Sobolev,* "Physics of planetary nebulae," Voprosy Kosmogonii, **VI**, 112–155, 1958.

Results of the paper [1] were included in the PhD thesis of V.V. Sobolev.

A short review of other papers by V.V. Sobolev devoted to physics of PNe is as follows. The diffusion of L_α radiation in nebulae and stellar envelopes was studied in [15]. The problem of the brightness of a spherical nebula was considered in [16]. The scattering of radiation of the central star in a spherical nebula was investigated by Kolesov and Sobolev in [7, 8].

Many problems devoted to physics of the nebulae were generalized in the famous Sobolev's Course in Theoretical Astrophysics [17].

3 Energy balance in gaseous nebulae

In his paper [14] V.V. Sobolev used the law of energy conservation in the following form:

$$n_1 \alpha \varepsilon = n_{\mathrm{e}} n^+ \sum_{i=1}^{\infty} \varepsilon_i + \mathsf{E} + n_1 n_{\mathrm{e}} \left(\gamma h\nu_0 + \sum_{i=2}^{\infty} D_i h\nu_{1i} \right). \tag{1}$$

In the left part of the equation the energy gained by electrons due to photoionization of the hydrogen atom is given, in the right part the energy losses are enumerated. Here n_1 is the population of the first atom level, α is the rate of ionization of the neutral hydrogen atom due to the radiation of the central star of the PN, and ε is the mean energy obtained by photoelectron after photoionization.

The value n_{e} is the electron number density, n^+ is the number density of ionized hydrogen atoms, ε_i is the part of energy lost by electrons at recombination to level i, E is the energy spent to emission in OIII lines N_1 ($\lambda\,5007$ Å) and N_2 ($\lambda\,5007$ Å, see Fig. 1, left panel), $h\nu_0$ is the energy of the hydrogen atom ionization from the ground level, γ is the rate of the H atom ionization by electron collisions, and D_i is the rate of energy lost by electrons due to collision excitation from

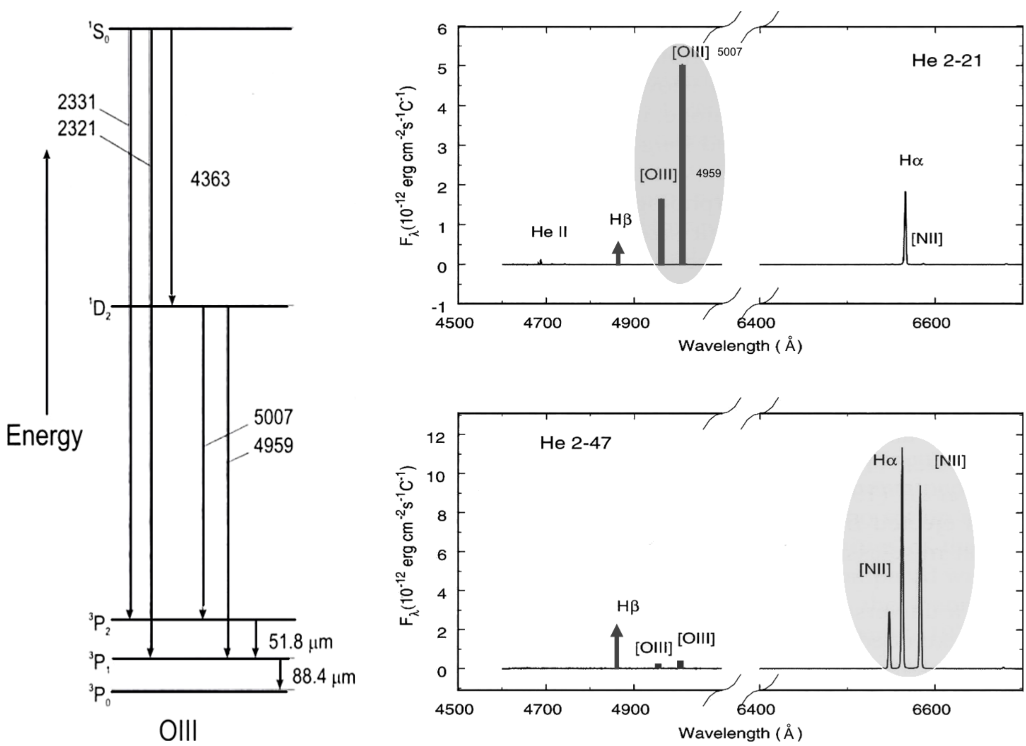

Figure 1: Left panel: ground and metastable OIII levels and corresponding forbidden lines. Right panel: spectra of the high and low excitation nebulae (based on Fig. 12.3 in [9]).

the ground level to level i (in units of $h\nu_1$ being the energy of excitation of the level i).

The left part of Eq. (1) was calculated by Sobolev, supposing that the emission of the central star (CS) of the PNe can be presented as the black-body emission with the temperature emission and for $\propto \nu^{-3}$ dependence of the photoionization cross sections of the H atoms with the ground level $i = 1$.

The same approximation for a dependence of the photoionization cross sections of the H atoms for an arbitrary level i was used to calculate the first term in the right part of Eq. (1).

In the time when Sobolev wrote his paper the values of effective cross sections for excitation of the upper levels of ion O^{2+} were unknown, so he estimated the value of E via the line intensity ratio $I(\mathrm{N}_2)/I(\mathrm{H}_\beta)$ supposing that the ratio $I(\mathrm{N}_1)/I(\mathrm{N}_2) = 3$. Then

$$\mathsf{E} = \int E dV = 4\frac{I(\mathrm{N}_2)}{I(\mathrm{H}_\beta)} A_{42} h\nu_{42} \int n_4 dV, \tag{2}$$

where A_{42} is the transition probability for line H_β, $h\nu_{42}$ is the energy of the transition $4 \to 2$ and n_4 is the population of the level $n = 4$ of hydrogen. It means that $\mathsf{E} \propto I(\mathrm{N}_2)/I(\mathrm{H}_\beta)$.

Table 1: Calculations by Sobolev in a comparison with the data of other authors

Nebular parameters						Contribution		
Name	$\frac{I(\mathrm{N}_2)}{I(\mathrm{H}_\beta)}$	$\frac{T_*^{VVS}}{10^3\mathrm{K}}$	$\frac{T_*}{10^3\mathrm{K}}$	$\frac{T_\mathrm{e}^{VVS}}{10^3\mathrm{K}}$	$\frac{T_\mathrm{e}}{10^3\mathrm{K}}$	Recom-bination	$\mathrm{N}_1+\mathrm{N}_2$	Excita-tion HI
IC 4593	1.7	25	28^a	13	6.0^c	0.25	0.60	0.15
NGC 6543	1.6	41	47^a	16	7.9^c	0.20	0.30	0.50
NGC 6572	2.4	48	66^a	18	8.9^c	0.15	0.40	0.45
NGC 6826	2.0	29	33^a	13	8.3^c	0.20	0.60	0.20
NGC 7009	3.1	45	98^b	15	6.5^c	0.15	0.55	0.30
NGC 7662	3.7	76	118^b	19	12.3^c	0.10	0.30	0.60

Notes: [a]Kaler, Jacobi (1991), [b]Capriotti, Kovach (1968), [c]Milanova, Kholtygin (2009).

The last term in Eq. (1) is determined by the value of n_1 which is the mean population of the ground level of hydrogen. For PNe, the ratio $n_1/n(\mathrm{H}) \ll 1$, where $n(\mathrm{H})$ is the full hydrogen number density. It means that the last term in Eq. (1) is proportional to n_1/n^+.

The final equation connecting the black-body temperature of the CS T_* and the mean electron temperature of the nebula T_e is as follows (Eq. 19 in [14]):

$$AT_* = BT_\mathrm{e} + C\,\frac{I(\mathrm{N}_2)}{I(\mathrm{H}_\beta)} + D\,\frac{n_1}{n^+}. \tag{3}$$

Here the ionization ratio n^+/n_1 can be determined using the equation of the ionization balance

$$\frac{n_\mathrm{e} n^+}{n_1} = W\sqrt{\frac{T_\mathrm{e}}{T_*}}\,\frac{(2\pi mkT_*)^{3/2}}{h^3}\,e^{-\frac{h\nu_0}{kT_*}}, \tag{4}$$

where W is the dilution factor, m is the mass of electron, k is the Boltzmann constant, h is the Planck constant, and $h\nu_0$ is the ionization potential for the ground level of H.

The coefficients A, B, C, D were calculated by Sobolev for $T_*/10^3\,\mathrm{K} \in [20, 80]$ and $T_\mathrm{e}/10^3\,\mathrm{K} \in [1, 50]$ (see Tables 1, 2 in [14]). He used these calculations to estimate the parameters T_e and $T*$ for selected PNe.

In Table 1 we list the values T_*^{VVS} and T_e^{VVS} obtained by Sobolev in [14] (columns 3 and 5) in a comparison with the data obtained in papers [4, 6, 12] (columns 4 and 6). In the columns 7–9 of Table 1 the contributions of different sources of cooling in the total cooling rate in Eq. (1) calculated by Sobolev are presented.

It is worth to note that the temperature of the central stars of the PNe obtained in the cited papers essentially exceeds the values given by Sobolev. Conversely, Sobolev's electronic temperatures for these PNe (in column 5) are significantly higher than the modern data by Milanova and Kholtygin [12] (column 6).

Table 2: Corrected cooling process contributions

Name	Contribution			$q(\mathrm{N}_1+\mathrm{N}_2)$
	Recombination	All collisions	Excitation HI	
IC 4593	0.13	0.87	–	0.66
NGC 6543	0.08	0.92	0.0002	0.32
NGC 6574	0.06	0.94	0.0003	0.31
NGC 6826	0.13	0.87	0.002	0.65
NGC 7009	0.03	0.97	–	0.24
NGC 7662	0.04	0.95	0.01	0.23

The main reason for this discrepancy in our opinion is underestimation of the energy loss due to excitation of the metastable levels of not only OIII but numerous ions of the other elements. If we look at Fig. 1 (right panel) we see that the fluxes of $\mathrm{N}_1+\mathrm{N}_2$ lines in the spectra of some nebulae are small in a comparison of the fluxes of other forbidden lines. It means that one has to add the new terms in the value E in Eq. (1).

The corrected energy balance equation (3) can be rewritten as

$$AT_* = BT_\mathrm{e} + E' + D\frac{n_1}{n^+}, \tag{5}$$

where E' is the corrected value of the energy losses due to excitation of *all* collisional transitions.

To estimate the value of E' we use the following procedure. Firstly, we take more exact than obtained by Sobolev values of T_* and T_e, which are given in the columns 4 and 6 of Table 1. Secondly, we calculate the coefficients A, B, D and the ratio n_1/n^+, using the data of Tables 1–4 in the paper [14] for these updated values of T_* and T_e.

Substituting those coefficients into Eq. (5), one can evaluate the full energy loss value E' and the ratio

$$q(\mathrm{N}_1+\mathrm{N}_2) = C\left(\frac{I(\mathrm{N}_2)}{I(\mathrm{H}_\beta)}\right)\Big/E',$$

the fraction of the energy excitation of $\mathrm{N}_1+\mathrm{N}_2$ lines in all collision energy losses E'.

In the columns 2–4 of Table 2 we give the corrected values of the relative contributions of the cooling processes for the same nebulae which are considered in Table 1. In the last column we present the ratio $q(\mathrm{N}_1+\mathrm{N}_2)$. Comparing Tables 1 and 2, we can conclude that the part of the energy losses which is spent to the excitation of hydrogen is negligible due to the lower electron temperatures than accepted in [14]. In the same time the recombination losses appear to be significantly less important than they were estimated by Sobolev. This result is in an agreement with Sobolev's main assumption that the collision processes give the most contribution to the energy loss by electron in the PNe.

4 Conclusions

Sobolev's works on physics of gaseous nebulae were among the first Foundation Stones of physics of planetary nebulae. Our review of Sobolev's work dedicated to physics of the nebulae showed that the main ideas proposed by Sobolev appear to be correct, but due to the poor knowledge of the atomic parameters in the time when Sobolev wrote his paper, the important corrections to the parameters of the PNe obtained by him have to be done.

References

1. *L.H. Aller, D.H. Menzel*, Astrophys. J., **102**, 239, 1945.
2. *V. Ambartsumian*, Tsirk. Pulkovo Obs., No. 6, 10, 1933.
3. *I.S. Bowen*, Astrophys. J., **67**, 1, 1928.
4. *E.R. Capriotti, W.S. Kovach*, Astrophys. J., **151**, 991, 1968.
5. *W. Huggins, W.A. Miller,* Phil. Trans. Roy. Soc., **154**, 437, 1864.
6. *J.B. Kaler, G.H. Jacoby*, Astrophys. J., **372**, 215, 1991.
7. *A.K. Kolesov, V.V. Sobolev*, Astrophys., **33**, 235, 1991.
8. *A.K. Kolesov, V.V. Sobolev*, Astrophys., **35**, 304, 1993.
9. *S. Kwok*, The Origin and Evolution of Planetary Nebulae. Cambridge: Cambridge University Press, 2000.
10. *S. Kwok*, Proc. IAU Symp., **283**, 1, 2012.
11. *D.H. Menzel*, Publ. Astron. Soc. Pacif., **38**, 295, 1926.
12. *Yu.V. Milanova, A.F. Kholtygin*, Astron. Lett., **35**, 518, 2009.
13. *C.D. Perrine*, Astron. Nachr., **237**, 89, 1929.
14. *V.V. Sobolev*, Trudy Astron. Obs. Leningr. Univ., **12**, 3, 1941.
15. *V.V.Sobolev*, Sov. Astron., **1**, 678, 1958 (original paper in Astron. Zh., **34**, 694, 1957).
16. *V.V. Sobolev*, Sov. Astron., **4**, 1, 1960.
17. *V.V. Sobolev*, Course in Theoretical Astrophysics. Moscow: Nauka, 1967 (1st edition), 1975 (2nd edition), 1985 (3rd edition).
18. *R.H. Stoy*, Mon. Not. Roy. Astron. Soc., **93**, 588, 1933.
19. *F.L. Whipple*, Harvard Coll. Obs. Bull., No. 908, 17, 1938.
20. *H. Zanstra*, Astrophys. J., **65**, 50, 1927.
21. *H. Zanstra*, Z. Astrophys., **2**, 1, 1931.

Diffuse Interstellar Bands Approaching Centenary

J. Krełowski[1]

E-mail: *jacek@umk.pl*

The paper presents in short the history of the investigations of diffuse interstellar bands (DIBs) – the longest standing unsolved problem of the whole spectroscopy. The importance of "peculiar" objects is emphasized as well as a search for the relations of DIBs to other (identified) interstellar spectral features. Some suggestions, concerning possible carriers of diffuse bands are presented as well.

1 Statement of the problem

The problem of DIBs is located in a broader subject matter of the physics and chemistry of the interstellar medium (ISM), which consists of atomic gas, molecules, and dust grains. The origin of these bands is as puzzling as since their first detection, more than 90 years ago.

DIBs appeared in the literature more than 90 years ago [1] as described in a nice, recent paper by McCall and Griffin [2]. However, the term "diffuse interstellar bands" was introduced later by P.W. Merrill (1938) who was the first to investigate these puzzling features systematically. At that time only six DIBs were known but their interstellar origin considered as certain. Fig. 1 demonstrates why the features are interstellar – they are stationary as well as NaI interstellar lines in the sharp contrast to stellar lines – and why they are known as "diffuse" – they are much shallower but broader than the NaI lines.

The application of solid state detectors to DIB observations led to discoveries of new features. Currently, the list of known DIBs contains 414 entries [3]; a majority of them – very shallow. Such a rich spectrum cannot share a common carrier; moreover the DIB profiles differ seriously from as narrow ones as about 1 Å (e.g. 6196) to more than 40 Å (e.g. 4430). They bear the name "diffuse" because their profiles are always broader than those of many of the well known atomic/molecular lines, even though the latter are much stronger (Fig. 1).

Nearly all conceivable forms of matter – from hydrogen anion to dust grains – have already been proposed as DIB carriers, so far with no generally accepted success. The abundance of elements in the Universe constrains the chemical composition of the DIB carriers. They ought to be built out of the most abundant elements: H, O, C, N, a small contribution of other elements also cannot be

[1] Center for Astronomy, Nicolaus Copernicus University, Toruń, Poland

V. Grinin et al. (eds) Radiation mechanisms of astrophysical objects. Yerevan: Edit Print, 2017, pp. 105–114.

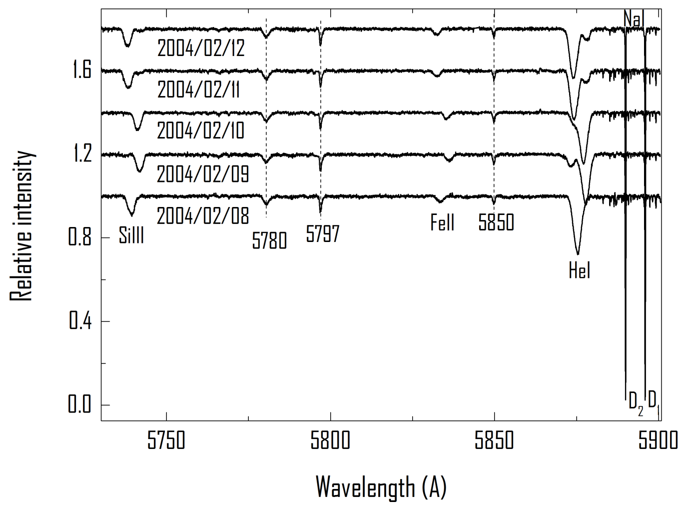

Figure 1: Interstellar NaI lines (right) and three diffuse bands in the spectra of HD 23180 – the spectroscopic binary with a 4.5 day period. Stellar lines (identified) perform the Doppler "dance". Note that strong interstellar NaI lines are narrower than the indicated DIBs.

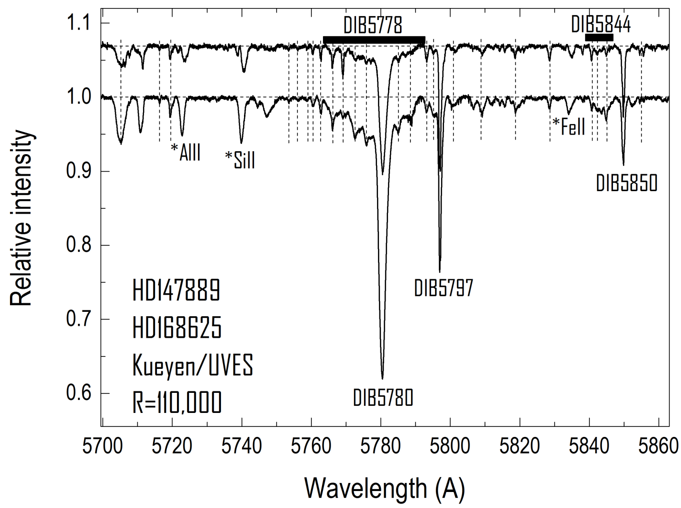

Figure 2: The spectral range in which M.L. Heger found the first two DIBs allows now to trace about 30 features, marked with vertical lines – a vast majority very shallow.

excluded. Among this group of elements carbon is in an exceptional position, since it can form a great number of stable compounds with a linear, planar and spherical structure. Bare carbon chains of 5 to 15 C atoms have been proposed as carriers of diffuse interstellar bands by Douglas [4]. Fulara et al. [5] and Freivogel et al. [6] later extended this hypothesis to the whole class of linear, unsaturated hydrocarbons. The interstellar medium (star forming regions) contains a lot of molecules based on carbon chain skeletons. Their vibrational and electronic transitions cause features in the spectral range full of diffuse bands. Apart from (hydro)carbon chains and polycyclic aromatic hydrocarbons (PAHs), also fullerenes (recently identified in circumstellar shells by [7]) fall in this category having features in visible and near infrared spectral ranges. Unfortunately, the existing spectra of the above mentioned molecules obtained in gas phase experiments (see for reviews [8, 9]) do not match the astrophysical ones. On the other hand, the spectra which have been acquired using the matrix isolation spectroscopy (MIS) cannot be directly compared to the astrophysical spectra. The features in MIS spectra are broadened and wavelength-shifted with respect to the gas phase (the magnitude of the shift remains unknown); the rotational structure is missing. However, the MIS spectra are necessary to determine relative strength ratios of molecular features as the CRDS technique (Cavity Ring Down Spectroscopy) – the method of acquiring gas-phase spectra of molecules – allows only to scan a single feature in a single experiment.

The fine structure (reminiscent of the rotational contours of bands of polyatomic molecules) has been detected in some DIBs [10, 11] giving a strong support to the idea of molecular origin of DIBs.

It is evident that the only way to identify the DIB carriers is to compare observed spectra with those of suspect molecules acquired in gas phase experiments. It is extremely important to keep in mind that what we observe are stellar spectra with interstellar features superimposed. No star is just a lamp, producing continuous spectrum. Stellar spectra contain many atomic lines originating in their atmospheres of the intensities depending on their temperatures, profiles depending on the luminosity class and widths – on rotational speed. This is why not every star allows to separate properly every interstellar feature from its spectrum. The additional problem is the likely present in a majority of targets Doppler splitting of interstellar features. DIB profiles modified in this fashion must not be compared to laboratory ones. This condition shrinks seriously the number of possible targets in which the DIB profiles can be used for such comparison.

The author is collecting high resolution echelle spectra of OB stars since 1993 using different instruments at both hemispheres. The latter is of basic importance for a reliable comparison between laboratory and astrophysical spectra. Very likely the recent attempts to identify neutral PAHs in translucent clouds [12, 13] failed because there are (most likely) a lot of different species in the space and thus abundances of individual PAHs are very small pushing their features below the detection level. Still much higher S/N ratio is necessary to discover ultraviolet PAH features. The very high S/N ratio spectrum of HD 169454 seems to contain the strongest feature of benzo[ghi]perylene (Fig. 3) – one of the investigated PAHs. The evident, neighbour C_3 band, is observed for the first time in this object [14]. High resolution echelle spectra allow to observe several spectral features of simple molecular species: CH, CH^+, CN, OH, OH^+, NH, C_2 and C_3; recently also SH [15]. It is interesting whether their abundance ratios are similar in all objects or not. The existing data suggest that CH and OH are closely related while NH and CH^+ behave in a different fashion [16, 17]. Let's emphasize that the above list allows

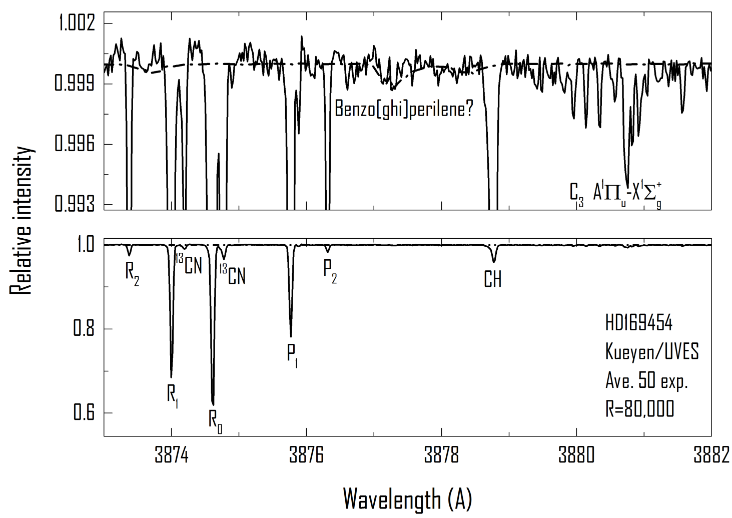

Figure 3: The extremely shallow feature in between of strong CN and CH bands, suggesting the presence of benzo[ghi]perylene in the spectrum of heavily reddened star. The dash-dot line is the laboratory spectrum, courtesy of F. Huisken.

to constrain chemistry of all most important elements: hydrogen, carbon, oxygen and nitrogen. The suggestion that profile widths of (some?) DIBs are related to rotational temperatures of simple carbon centrosymmetric species [18] needs a broader survey.

A comparison of band strength measurements, DIB profile details and their mutual relations require very high resolution, S/N ratio and a broad wavelength range. The necessary observations are very time-consuming and require well-designed procedures of data acquiring and reducing.

2 Families of diffuse bands?

The term "families" was used for the first time in the literature in relation to DIBs by Krełowski and Walker [19]. High resolution and high SNR spectra demonstrated that the strength ratio of the major DIBs: 5780 and 5797 changes from object to object. A similar result, confirming the variable DIB strength ratio was published soon after by Josafatsson and Snow [20] confirming that they are not of common origin but belong to different "families" considered as sets of features of common origin. Since 1975 the set of known DIBs was reasonably large [21] which also could suggest diverse origin of the whole DIB spectrum.

The two first objects, in which the variable ratio of major DIBs was observed as early as 1983, are HD 147165 (σ Sco) and HD 149757 (ζ Oph). The result was, however, published a couple of years later [22] for it looked incredible at that time. The terms σ and ζ type clouds, popular now, are rooted in that "ancient" project. The objects were later observed several times and the σ and ζ type clouds were connected not only to the 5780/5797 ratio but also to the shapes

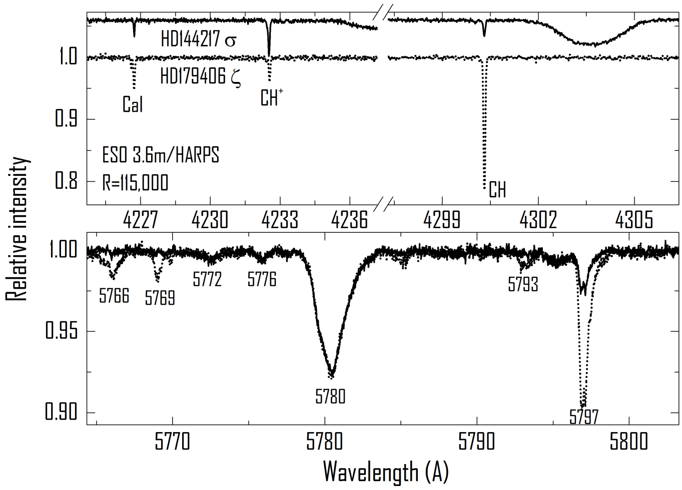

Figure 4: Major DIBs (lower panel) and the bands of simple interstellar radicals, observed in the spectra of HD 144217 and HD 179406 – the typical of σ and ζ type clouds. Note the identical intensity and profile of the 5780 DIB.

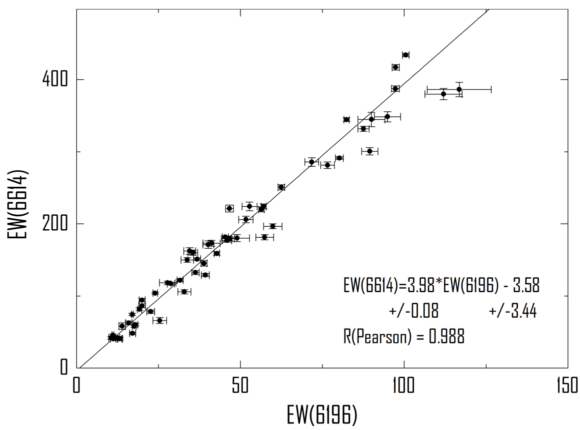

Figure 5: The nearly perfect correlation of the strengths of 6196 and 6614 DIBs.

of extinction curves (see [23]) and to the relative abundances of simple interstellar radicals [24]. Both DIBs and bands carried by simple molecules are depicted in Fig. 4, presenting the two σ and ζ type clouds of similar $E(B-V)$.

Naturally the very first idea was that one "family" members should share the carrier and thus – should be of constant strength ratio. The first DIB survey [25] found a pair that correlates almost perfectly: 6196 and 6614. The former is quite narrow while the latter is quite broad which does not support the idea of common origin. Their equivalent width ratio is nearly 4. This tight correlation was confirmed later by other teams, e.g [26] – it is thus established beyond a reasonable doubt. However, Galazutdinov et al. [11] demonstrated that while the strengths of the two DIBs are well correlated, their FWHMs (full-width half-maxima) are not. Figure 5 presents the above mentioned tight correlation based on spectra from three major world spectrographs: HARPS fed with the

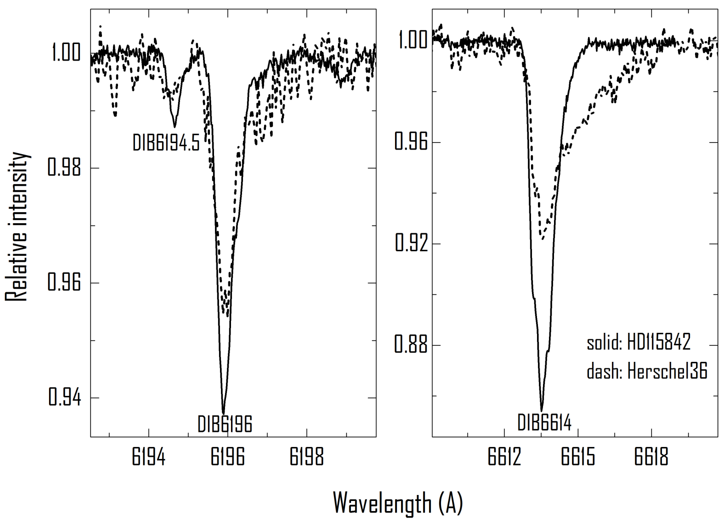

Figure 6: The lack of correlation between FWHM's of 6196 and 6614 DIBs. Note that also some differences of the strength ratio may be physically grounded.

3.6m ESO LaSilla telescope, UVES – attached to the Kueyen mirror of the VLT at Paranal and BOES – fed with the national Korean telescope at Bohyunsan. The very high correlation coefficient is shown. It is, however, a necessary but not a sufficient condition. Analyzing a spectrum of the Herschel 36, it is possible to find more spectacular evidence that FWHMs of the two DIBs do not behave in unison (Fig. 6). Moreover, the scatter, seen in Fig. 5, is very likely caused by different physical conditions inside individual clouds – not by just the measurements' errors.

3 Rest wavelengths

Rest wavelengths of DIBs are necessary to identify these puzzling features. However, having no identification we must not have the laboratory wavelengths of any spectral line or band. It is natural that the observed wavelengths of interstellar features are Doppler shifted because of the relative motions of interstellar clouds, the Sun and the Earth. One can shift the wavelength scale of any spectrum to that of some interstellar identified line; this may allow to determine the laboratory wavelengths of unidentified features providing they share the place of origin with the chosen identified line. This may be complicated because not all identified interstellar lines or bands share the same radial velocity.

Seemingly the only proper way to determine rest wavelengths of DIBs is to find an object (or a couple of objects) where radial velocities of all identified lines or bands are identical and their profiles – free of the Doppler splitting. Such objects are very scarce. They should be reasonably bright to allow acquiring high S/N spectra and reasonably heavily reddened to make the tracing of weak DIBs possible. The additional difficulty follows the fact that DIB profiles are not just Gaussians and thus their central wavelengths may not coincide in different publications. This is broadly discussed in the paper by Bondar [27] where the rest wavelengths of 336 DIBs are determined using high quality spectra of 10 stars. However, even this method may not always lead to proper results. The example is the Orion Trapezium [28] where the observed DIBs are apparently red-shifted.

There is no explanation of this effect. Anyway it creates possible doubts on how far the wavelengths of DIBs, shifted to the rest wavelength frames of interstellar lines, are equal to the laboratory ones.

4 Profiles of diffuse bands

As mentioned above, the intrinsic profiles of diffuse bands are not just Gaussians; the profiles are not only quite broad but also asymmetric with possible substructures inside. Since the first such analysis [29] it was established that practically all narrow diffuse bands demonstrate some substructure patters, suggesting their molecular origin. It was demonstrated clearly in the paper by Galazutdinov et al. [11]. The profiles of very well correlated 6196 and 6614 DIBs apparently change from object to object where no Doppler splitting is observed in identified lines. The influence of the Doppler splitting on the observed DIB profiles was demonstrated, e.g., by Westerlund and Krełowski [30]. This mechanical broadening makes difficult a comparison of observed and laboratory DIB profiles.

It seems reasonable that changes of DIB profiles are results of different rotational temperatures of their carriers if the latter are molecules as well. It is much easier to find differences in rotational temperatures of centrosymmetric molecules as such temperatures may cover a very broad range [31].

Herschel 36 is a very specific object – the only such one in the sky. Oka et al. [32] found the CH and CH^+ molecules in its spectrum to be rotationally excited. The exceptionally high rotational temperatures of the simple, polar radicals are apparently related to severely broadened profiles of some DIBs (Fig. 7). However, not all profiles are broadened; for example that of the 5850 DIB is free of any visible broadening.

Another unique object in the sky is HD 34078 (AE Aur). Adamkovics et al. [31] found the exceptionally high rotational temperature of the C_3 molecule in this object. The object seems extremely interesting as the spectral features in its spectrum, carried by simple interstellar radicals, decline with time. Despite of this the profiles of diffuse bands seem to be broadened and their gravity centers – blue-shifted [33]. Also in this case one can expect that the rotational temperatures of the DIB carriers may be responsible for the observed changes of profiles.

The star taken for comparison is HD 27778. Apparently, the 5797 profile resembles that, observed by Oka et al. [32] in 9 Sgr. It is interesting that the DIB is broadened in HD 34078 as well but it looks also blue-shifted. The rotational components of CH^+ and CH are not observed in HD 34078 and so the rotational temperature of these species is apparently lower than in Herschel 36.

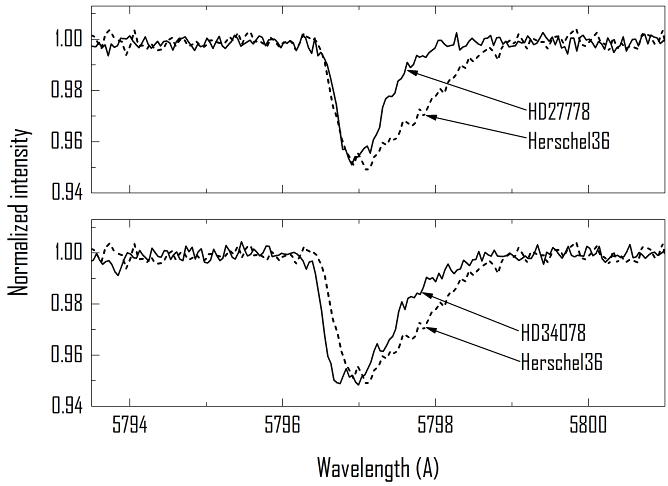

Figure 7: 5797 DIB profiles broadened in the spectra of Herschel 36 and HD 34078. The comparison of HD 27778 with Herschel 36 closely resembles Fig. 3 of [32]. Apparently the DIB is broadened in HD 34078 but not as much as in Herschel 36. The spectra of HD 34078 and HD 27778 are from MIKE ($R = 67\,000$) while that of Herschel 36 from Feros ($R = 48\,000$). All spectra are shifted to the rest wavelength velocity frame using the KI 7699 Å line.

"Peculiar" cases, like AE Aur or Herschel 36, are extremely interesting because they do reflect some specific situations which can take place only in individual clouds (likely homogeneous environments). Unfortunately such cases are extremely rare; it is of basic importance to hunt for more such "peculiar" objects – perhaps they will allow to understand the physics and chemistry leading to the formation of the DIB spectrum.

5 Identification propositions

The first proposition of a DIB identification, but signed with a question mark, is the CH_2CN^- molecule proposed as the carrier of the 8037 Å DIB by Cordiner and Sarre [34]. This feature is located in the wavelength range severely contaminated with telluric lines and fringes. Thus it is very difficult to check whether the identification is reliable because the profile of it is clearly seen only in a few objects and no more its features are proposed.

Recently we found a very weak DIB which coincides with the electronic, gas-phase band of HC_4H^+; this finding [35] supports DIB molecular origin. The identification was disputed by Maier et al. [36]; this fact clearly demonstrates the necessity of close cooperation between experimentalists and observers. The lack of the latter leads to obvious confusions. The wavelength of the above mentioned feature may be a bit floating due to different rotational temperature of the carrier. Unfortunately, the band is so weak that a proper statistics of observations is hardly available.

Another overlap between a lifetime broadened absorption spectrum, recorded through a hydrocarbon plasma and a stronger DIB at 5450 Å was reported by [37]; an identification of the carrier was not possible yet. If l-C_3H_2 can produce the 5450 Å DIB, as proposed by Maier et al. [38] then the carrier is unacceptably abundant; moreover the second l-C_3H_2 feature, near 4883 Å is clearly of another origin [39].

The recently published by Campbell et al. [40] gas phase spectra of the $C_{60}{}^{+}$ reactivated the dormant idea of this species to be the carrier of two near infrared DIBs: 9577 and 9632. According to the authors the cation of $C_{60}{}^{+}$ exhibits four relatively strong spectral lines centered at 9365.9, 9428.5, 9577.5 and 9632.7 Å with relative intensity 0.2, 0.3, 1.0 and 0.8, respectively, and the wavelength precision not worse than 0.1Å. However, the authors did not collect big enough sample of spectra allowing a comparison with the laboratory data. The strength ratio of both strong, observed features may seriously differ from the laboratory predictions; moreover the ratio is apparently variable if observed in a pretty big sample of targets. Also the rest wavelengths of both DIBs do not match the laboratory ones inside the possible errors.

Acknowledgments. The author is very indebted to Dr. G.A. Galazutdinov for very helpful discussions. The paper was financially supported by the grant 2015/17/B/ST9/03397 of the Polish National Science Center.

References

1. *M.L. Heger*, Lick Obs. Bull., **10**, 141, 1922.
2. *B.J. McCall, E. Griffin*, Proc. Roy. Soc. A, **469**, 20120604, 2013.
3. *L.M. Hobbs, D.G. York, J.A. Thorburn et al.*, Astrophys. J., **705**, 32, 2009.
4. *A.E. Douglas*, Nature, **269**, 130, 1977.
5. *J. Fulara, D. Lessen, P. Freivogel, J.P. Maier*, Nature, **366**, 439, 1993.
6. *P. Freivogel, J. Fulara, J.P. Maier*, Astrophys. J., **431**, 151, 1994.
7. *J. Cami, J. Bernard-Salas, E. Peeters, S.E. Malek*, Science, **329**, 1180, 2010.
8. *E.B. Jochnovitz, J.P. Maier*, Ann. Rev. Phys. Chem., **59**, 519, 2008.
9. *H. Linnartz*, in Cavity Ring-down Spectroscopy Techniques and Applications. Eds. G. Berden, R. Engeln. Wiley-Blackwell, 2009, p. 145.
10. *T.H. Kerr, R.E. Hibbins, S.J. Fossey et al.*, Astrophys. J., **495**, 941, 1998.
11. *G.A. Galazutdinov, C. Moutou, F. Musaev, J. Krełowski*, Astron. Astrophys., **384**, 215, 2002.
12. *F. Salama, G. Galazutdinov, L. Biennier et al.*, Astrophys. J., **728**, 154, 2011.
13. *R. Gredel, Y. Carpentier, G. Rouill et al.*, Astron. Astrophys., **530**, 26, 2011.
14. *M.R. Schmidt, J. Krełowski, G.A. Galazutdinov et al.*, Mon. Not. Roy. Astron. Soc., **441**, 1134, 2014.

15. *D. Zhao, G. Galazutdinov, H. Linnartz, J. Krełowski*, Astron. Astrophys., **579**, 1, 2015.
16. *T. Weselak, G. Galazutdinov, Y. Beletsky, J. Krełowski*, Mon. Not. Roy. Astron. Soc., **402**, 1991, 2010.
17. *T. Weselak, G. Galazutdinov, Y. Beletsky, J. Krełowski*, Astron. Astrophys., **499**, 783, 2009.
18. *M. Kazmierczak, P. Gnaciński, M.R. Schmidt et al.*, Astron. Astrophys., **498**, 785, 2009.
19. *J. Krełowski, G.A.H. Walker*, Astrophys. J., **312**, 860, 1987.
20. *K. Josafatsson, T.P. Snow*, Astrophys. J., **319**, 436, 1987.
21. *G.H. Herbig*, Astrophys. J., **196**, 129, 1975.
22. *J. Krełowski, B.E. Westerlund*, Astron. Astrophys., **190**, 339, 1988.
23. *E.L. Fitzpatrick, D. Massa*, Astrophys. J., **663**, 320, 2007.
24. *J. Krełowski, T.P. Snow, C.G. Seab, J. Papaj*, Mon. Not. Roy. Astron. Soc., **258**, 693, 1992.
25. *C. Moutou, J. Krełowski, L. d'Hendecourt, J. Jamroszczak*, Astron. Astrophys., **351**, 680, 1999.
26. *B.J. McCall, M.M. Drosback, J.A. Thorburn et al.*, Astrophys. J., **708**, 1628, 2010.
27. *A.V. Bondar*, Mon. Not. Roy. Astron. Soc., **423**, 725, 2012.
28. *J. Krełowski, G.A. Galazutdinov, G. Mulas et al.*, Mon. Not. Roy. Astron. Soc., **451**, 3210, 2015.
29. *B. Westerlund, J. Krełowski*, Astron. Astroph., **218**, 216, 1988.
30. *B. Westerlund, J. Krełowski*, Astron. Astroph., **189**, 221, 1988.
31. *M. Adamkovics, G.A. Blake, B.J. McCall*, Astrophys. J., **595**, 235, 2003.
32. *T. Oka, D.E. Welty, S. Johnson et al.*, Astrophys. J., **773**, 42, 2013.
33. *G.A. Galazutdinov, G. Manico, J. Krełowski*, Mon. Not. Roy. Astron. Soc., **366**, 1075, 2006.
34. *M.A. Cordiner, P.J. Sarre*, Astron. Astrophys., **472**, 537, 2007.
35. *J. Krełowski, Y. Beletsky, G. Galazutdinov et al.*, Astrophys. J. Lett., **714**, L64, 2010.
36. *J.P. Maier, S. Chakrabarty, F.J. Mazzotti et al.*, Astrophys. J. Lett., **729**, L20, 2011.
37. *H. Linnartz, N. Wehres, H. van Winckel et al.*, Astron. Astrophys., **511**, 3, 2010.
38. *J.P. Maier, G.A.H. Walker, D.A. Bohlender et al.*, Astrophys. J., **726**, 41, 2011.
39. *J. Krełowski, G. Galazutdinov, R. Kołos*, Astrophys. J., **735**, 124, 2011.
40. *E.K. Campbell, M. Holz, D. Gerlich, J.P. Maier*, Nature, **523**, 322, 2015.
41. *M. Kazmierczak, M.R. Schmidt, G.A. Galazutdinov et al.*, Mon. Not. Roy. Astron. Soc., **408**, 1590, 2010.

Interstellar Extinction and Polarization and Star Formation in Dark Clouds

A.K. Sen[1], V.B. Il'in[2,3], M.S. Prokopjeva[2], N.V. Voshchinnikov[2], R. Gupta[4]

E-mail: *asoke.kumar.sen@aus.ac.in*

Polarimetry of stars background to dark clouds provides an important tool to map the magnetic field in the cloud. These polarimetric measurements have significance as the magnetic field plays a key role in star formation dynamics. However, simultaneous interpretation of extinction and polarization for such clouds poses problems for theoreticians. Some of these problems are discussed in the present work and possible explanations are provided.

1 Introduction

It is well known that light from celestial sources, when passes through the interstellar medium, gets polarized due to the aligned dichroic interstellar dust grains. At times, the light passes through denser parts of the interstellar medium which usually contain *interstellar clouds*. Some of these clouds are undergoing gravitational collapse and may form stars. The amount of the polarization caused by such intervening clouds provides valuable information and acts as a good diagnostic to understand various processes associated with star formation.

The dichroic grains present in such clouds generally get aligned by various mechanisms, where the magnetic field is an important component [1]. The same magnetic field also plays a key role in the dynamics of star formation and helps in deciding the shape of the clouds [2]. Some of these clouds have rotations, which together with the magnetic field sometimes impede the gravitational collapse [3]. The grains, on the other hand, absorb radiation at shorter wavelengths and *reradiate in the infrared,* helping the energy balance mechanism. The thermally re-radiated emission also shows polarization [4, 5].

In our galaxy we have many small compact dark clouds (known as Bok globules), undergoing gravitational collapse, that may form low mass stars [6, 7]. They mainly contain molecular gas and dust, having the gas temperature $\sim$10–30 K and density $\sim 10^4$ cm^{-3}, the total mass about 10–100 $M_\odot$ and the size

[1] Dept. of Physics, Assam University, India
[2] St. Petersburg University, Russia
[3] Pulkovo Observatory, Russia
[4] IUCAA, India

V. Grinin et al. (eds) Radiation mechanisms of astrophysical objects. Yerevan: Edit Print, 2017, pp. 115–120.

about 1–2 pc. The role of gravity is to be understood in a situation, where we have thermal outward pressure, turbulence, rotation and the magnetic field (also electrostatic charging [8] and so on). Towards the cloud core the total extinction can be as large as $A_V > 25$ mag, whereas in the outer periphery, where most of the optical polarimetric observations are carried out, $A_V < 5$ mag (see, e.g., [9]).

With this background, over the last few decades many dense interstellar clouds were astronomically observed by various groups in polarimetry, to understand the star formation processes in them. In spite of that, we still have a number of unresolved critical issues associated with such observation and analysis, namely: *Are background star polarimetry and re-emission polarimetry really capable of estimating magnetic field? Why the extinction data most often do not seem to be related to the polarization data? How interstellar polarization measurement is related to background star polarimetry?*

In this paper, we go through some of these issues and draw conclusions.

2 Interstellar extinction and polarization

The interstellar extinction and polarization over a wide wavelength range have been studied by many authors, which helped to characterize the grains' composition, shape and size, and also the number density distribution and the magnetic field. For instance, Gupta et al. [10] considered mixtures of silicate and graphite oblate spheroidal grains of the aspect ratio $a/b = 1.33$ within the wavelength range 0.1–3.4 μm to simulate the interstellar extinction. On the other hand, Das et al. [11], considering homogenous carbonaceous and silicates spheroids containing C, O, Mg, and Fe and the imperfect Davis–Greenstein (DG) alignment mechanism, explained the interstellar extinction as well as polarization curves. Voshchinnikov and Henning [12] also made such studies with a special emphasis on the dust composition and found that the dust phase abundance of Si, Fe, Mg played an important role to decide some of the observed phenomena. Many other aspects of interpretation of the interstellar polarization and extinction observations have been recently reviewed in [13].

3 Background star extinction and polarization for dark clouds

For the stars background to diffuse clouds, we know that the dichroic grains absorb optical radiation from background stars, resulting in the optical polarization. The same set of dust reradiates thermally resulting in the sub-mm and IR polarization. In past, Vrba et al. [14], Joshi et al. [15], Goodman et al. [16], Myers and Goodman [17], Kane et al. [18], Sen et al. [19], Whittet [20], Andersson and Potter [21] and other authors made such optical polarimetric studies. The works on polarization by the thermal re-emission were reported, e.g., by Ward-Thompson et al. [22] and Henning et al. [23] among others.

The background star polarimetric results are generally analyzed in the same way as interstellar polarization values. But since sometimes we encounter many problems while interpreting results of background star polarimetry, it appears that, understanding the processes in the background star polarimetry is not as simple as understanding the interstellar polarization.

Some of the observations of the background star polarization need attention:

1. Optical and NIR polarimetry does not show an increase in the polarization degree as one goes closer to the center of a dark cloud (signifying an increase in the optical depth) (e.g., [15, 9]).
2. The extinction and corresponding polarization for a set of background stars should be related for dark clouds, but most of the recent studies show they are not. So, Goodman et al. [24] questioned the validity of this technique to study the magnetic fields within the clouds.
3. For a set of eight clouds, Sen et al. [25] found that the perfect DG mechanism could not explain the observed polarization. Many other investigators also noted that the DG mechanism predicted much higher values of polarization than the actually observed ones. The question naturally arises, is polarization in the optical caused by grains which are aligned by DG mechanism or other processes? If we understand the process, then we can map the magnetic field more confidently.
4. Again far-IR observation gives polarization values which are consistent with the thermal re-emission from grains [27, 26].
5. Not only that, these far-IR polarization values are also consistent with the absorption polarization in the optical region. The polarization in this region comes from the low density region ($A_{\rm V} \sim$ 1–5 mag) of the cloud (near the periphery), while in the sub-mm domain (850 μm) does from near the core ($A_{\rm V} \sim$ 10–100 mag). The optical polarization direction is parallel to the magnetic field. The sub-mm polarization is due to the preferential emission from aligned elongated grains and should be *perpendicular* to the magnetic field. A comparison of the optical (from the Indian telescope) and sub-mm (from the SCUBA data archive) polarization vectors confirmed these findings [27]. Recent Planck data give a deeper insight on the relation between the sub-mm and visual polarization [5].
6. As found by Sen et al. [25] from a study of eight clouds, turbulence within the cloud was influencing (rather disturbing) the grain alignment and this could be modeled through a mathematical relation (see Fig. 1).
7. As an exception to point (2) above, Sen et al. [28] found that at least for some clouds, there was a positive correlation between polarization and extinction.

Basing on points (1) to (3), one could say that the intervening cloud has no role in the polarization that we observe for the stars background to the cloud. But in that case, we can not explain the points (4) to (6) listed above, which suggests that the polarization observed for background stars must have something intrinsic to the cloud.

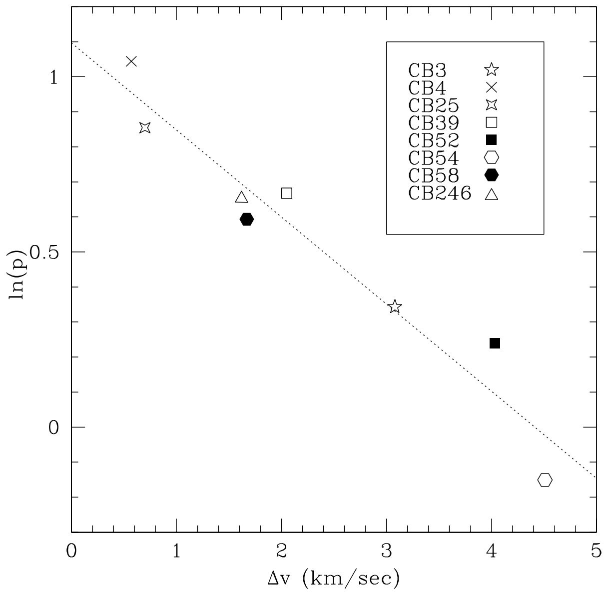

Figure 1: The log of the average observed polarization $\ln(p)$ against the turbulence velocity Δv (in km/s) for different clouds according to [25]. The line of the best fit $\ln(p) = 1.08 - 0.24\,\Delta v$ is shown.

There *exist* various possibilities which can explain the present situation. There are now doubts that the DG-like mechanisms play a role as large as thought earlier, and many researchers believe that the most important aligning force could be radiative torques [29]. However, it does not exclude the role of other mechanisms which can align grains.

It is very possible that some particular mechanism works in some parts of the cloud as compared to others. Also a particular alignment mechanism may be more effective for grains with a particular size and composition. Voshchinnikov [13], while working on the interstellar polarization, discussed such possibilities. And for dark clouds, it may be even more complicated. Within such a cloud, along the line of sight different values of the parameters of the magnetic field (or other aligning forces) are possible.

As listed in [30], a set of conditions should be fulfilled to get polarization out of aligned grains. If these conditions are not satisfied, we can get extinction, but not polarization.

Any misadjustment in these conditions should result in a poor correlation between polarization and extinction. The grain shape, size, magnetic properties (composition), alignment procedure are important parameters and some of these physical properties should vary within the clouds. And recent studies of extinction law, scattered light and sub-mm emissivity have already inferred changes in dust properties with an increase of depth inside a cloud (see [31] and references therein). So, the polarization observed for stars background to dark clouds may appear to be quite different from the polarization observed for the diffuse interstellar medium.

4 Conclusions

We can conclude as follows:

1. It is clear that the polarization values observed for stars behind dark clouds are influenced by the physical processes within these clouds.
2. However, the physical processes responsible for producing the polarization *in* the clouds are not well understood.
3. The processes producing the interstellar polarization and the polarization of background star radiation in dark clouds are definitely not the same.
4. The processes responsible for the polarization in dark clouds should be *more* clearly understood, as we find the situation is not as simple as in the interstellar medium. Only after this, we can use in the full manner the background star polarimetry to investigate star formation processes in dark clouds.

Acknowledgments. The authors acknowledge a partial support of the work by the grants of RFBR 16-02-00194, DST-RFBR 16-52-45005 and SPbGU 6.38.18.2014.

References

1. *R.M. Crutcher*, Ann. Rev. Astron. Astrophys., **50**, 29, 2012.
2. *H.-B. Li, A. Goodman, T.K. Sridharan et al.*, In: Protostars & Planets, VI. Tucson: Univ. Arizona Press, 2014, p. 101.
3. *P. Hennebelle, C. Charbonnel (eds.)*, Angular Momentum Transport during the Formation and Early Evolution of Stars. EAS Publ. Ser., **62**, 2013.
4. *B.T. Draine, A. Fraisse*, Astrophys. J., **696**, 1, 2009.
5. *Planck Collaboration*, Astron. Astrophys., **576**, A106, 2016.
6. *B.J. Bok, E.F. Reilly*, Astrophys. J., **105**, 255, 1947.
7. *B.J. Bok*, Astron. J., **61**, 309, 1956.
8. *C.B. Dwivedi, A.K. Sen, S. Bujarbarua*, Astron. Astrophys., **345**, 1049, 1999.
9. *V.B. Il'in, Y.S. Efimov, T.N. Khudyakova, M.S. Prokopjeva*, 2016, this conference.
10. *R. Gupta, T. Mukai, D.B. Vaidya et al.*, Astron. Astrophys., **441**, 555, 2005.
11. *H.K. Das, N.V. Voshchinnikov, V.B. Il'in*, Mon. Not. Roy. Astron. Soc., **404**, 265, 2010.
12. *N.V. Voshchinnikov, Th. Henning*, Astron. Astrophys., **517**, A45, 2010.
13. *N.V. Voshchinnikov*, J. Quant. Spectrosc. Rad. Transf., **113**, 2334, 2012.
14. *F.J. Vrba, G.V. Coyne, S. Tapia*, Astrophys. J., **243**, 489, 1981.

15. *U.C. Joshi, P.V. Kulkarni, H.C. Bhatt et al.*, Mon. Not. Roy. Astron. Soc., **215**, 275, 1985.
16. *A.A. Goodman, R.M. Crutcher, C. Heiles et al.*, Astrophys. J. Lett., **338**, L61, 1989.
17. *P.C. Myers, A.A. Goodman*, Astrophys. J., **373**, 509, 1991.
18. *B.D. Kane, D.P. Clemens, R.W. Leach, R. Barvainis et al.*, Astrophys. J., **445**, 269, 1995.
19. *A.K. Sen, R. Gupta, A.N. Ramaprakash, S.N. Tandon*, Astron. Astrophys., **141**, 175, 2000.
20. *D.C.B. Whittet, P.A. Gerakines, J.H. Hough, S.S. Shenoy*, Astrophys. J., **547**, 872, 2001.
21. *B.-G. Andersson, S.B. Potter*, Astrophys. J., **665**, 369, 2007.
22. *D. Ward-Thompson, J. Kirk, R. Crutcher et al.*, Astrophys. J. Lett., **537**, L135, 2000.
23. *Th. Henning, S. Wolf, R. Launhardt, R. Waters*, Astrophys. J., **561**, 871, 2001.
24. *A.A. Goodman, T.J. Jones, E.A. Lada, P.C.Myers*, Astrophys. J., **448**, 748, 1995.
25. *A.K. Sen, T. Mukai, R. Gupta, H.S. Das*, Mon. Not. Roy. Astron. Soc., **361**, 177, 2005.
26. *B.T. Draine*, IAU Gen. Assembly, Meet. #29, id.2253136, 2015.
27. *D. Ward-Thompson, A.K. Sen, J.M. Kirk, D. Nutter*, Mon. Not. Roy. Astron. Soc., **398**, 394, 2009.
28. *A.K. Sen, V.F. Polcaro, I. Dey, R. Gupta*, Astron. Astrophys., **522**, 45, 2010.
29. *B-G. Andersson, A. Lazarian, J.E. Vaillancourt*, Ann. Rev. Astron. Astrophys., **53**, 501, 2015.
30. *N.V. Voshchinnikov, T. Henning, M.S. Prokopjeva, H.K. Das*, Astron. Astrophys., **541**, A52, 2012.
31. *J.B. Foster, K.S. Mandel, J.E. Pineda et al.*, Mon. Not. Roy. Astron. Soc., **428**, 1606, 2013.

Estimates of Brightness Temperatures for Maser Sources of the Galaxy Observed by Space Interferometer "RadioAstron"

N.N. Shakhvorostova[1], A.V. Alakoz[1], A.M. Sobolev[2]
on behalf of the RadioAstron maser survey team

E-mail: *nadya@asc.rssi.ru*

The ultra-high angular and high spectral resolutions of RadioAstron provide tight limits on the sizes of the most compact maser spots and the estimates of their brightness temperatures. We present the results of the maser survey obtained by RadioAstron during the first four years of operation. Very compact features with angular sizes not exceeding about 20–60 micro-arcseconds have been detected in star-forming regions. Corresponding linear sizes are about 5–10 millions of kilometers. Brightness temperatures for a number of maser sources are estimated. Estimates of the brightness temperatures provide the values from $\sim10^{14}$ to $\sim10^{16}$ K.

1 Observations of masers with RadioAstron

Maser sources represent one of the main targets of the RadioAstron (RA) science program along with active galactic nuclei and pulsars. The RadioAstron project allows us to observe maser emission in one quantum transition of water at 22.235 GHz and two transitions of hydroxyl at 1.665 and 1.667 GHz. Water and hydroxyl masers are found in star-forming regions of our and nearby galaxies, around mass-loosing evolved stars, and in accretion discs around super-massive black holes in external galaxies.

Masers have small angular sizes (a few milli-arcsec and smaller), very high flux densities (up to hundreds of thousand Jy), and small line widths (normally about 0.5 km/s and smaller). Due to that masers proved to be precise instruments for studies of kinematics and physical parameters of the objects in our and other galaxies.

The space radio interferometer RadioAstron provides a record of high angular resolution, in some cases reaching a few tens of micro-arcseconds. This provides tight limits on the sizes of the most compact maser spots and estimates of their brightness temperatures, which are necessary input for the studies of the pumping mechanisms.

[1] Astro-Space Center of LPI RAS, Russia
[2] Ural Federal University, Russia

V. Grinin et al. (eds) Radiation mechanisms of astrophysical objects. Yerevan: Edit Print, 2017, pp. 121–126.

Typical values of the minimal flux density detectable with RA for the water masers at 22 GHz and hydroxyl masers at 1.665/1.667 GHz are 15 Jy and 3.5 Jy, respectively. These values were calculated for a typical line width of 0.1 km/s and coherent accumulation time of 100 s and 600 s for 22 GHz and 1.665/1.667 GHz, respectively. So, the sensitivity in Jy for hydroxyl masers is better than for water masers. Anyhow, when we use the large ground-based antenna, for example 100-m GBT, and the source has wide line, RA proved ability to detect 3–4 Jy water maser source.

2 Statistics of maser observations for the first 4 years of operation

2.1 Maser observation program

The goal of the scientific program for the study of cosmic masers using space interferometer RadioAstron was observations of maser emission in quantum transitions of water at frequency 22 GHz and hydroxyl at frequencies 1.665 and 1.667 GHz. During the period from November 2011 to May 2012 interferometric mode of RA operation was tested. For that purpose a number of bright quasars and the brightest and most compact sources of maser emission were selected [1]. Basic conditions for choosing these sources were the existence of details that remain compact (i.e. unresolved) on the longest baseline projections and the highest brightness temperatures measured during VLBI and VSOP surveys. The first positive detections of maser sources by space interferometer were achieved for W51 (water) and W75N (hydroxyl) in two sessions in May and July 2012. Baseline projections were 1.0–1.5 and 0.1–0.8 Earth diameters (ED), respectively. Later, more sophisticated data analysis led to even more positive results in these test sessions: compact water maser features were detected in W3 IRS5 and W3(OH) in two sessions in February 2012. Baseline projections were 3.7–3.9 ED.

After the first successful tests the early science program started. The main purpose of these observations was to obtain first astrophysical results and measurements of the main parameters of the operating interferometer. List of observed sources has been significantly expanded, objects of other types were included in addition to the star-forming regions. Stellar masers in S Per, VY CMa, NML Cyg, U Her and extragalactic masers in Circinus and N113 were observed. It was proved that RadioAstron can observe cosmic masers with very high spectral resolution. This was not obvious at the beginning, indicates presence of the ultra-fine structure in the maser images, and that interstellar scattering does not prevent observations of masers in the galactic plane [1]. Positive detections for stellar and extragalactic masers were not obtained during the early science program.

The early science program was followed by the key and general research programs which were conducted (and the general program continues at the moment) on the basis of the open call for proposals received from research teams around the world. Details of the preparation and the conditions of the

Table 1: Maser sources detected on the space–ground baselines

Source	Observed line(s)	Projected baseline length, ED
W3 IRS5	22 GHz (H_2O)	2.5–2.8; 3.5; 3.9; 5.4; 6.0
W51_E8	22 GHz (H_2O)	0.4–2.3; 1.3; 1.4–1.8
Cepheus A	22 GHz (H_2O)	0.9–1.7; 1.1; 3.1–3.5
W49N	22 GHz (H_2O)	2.2–3.0; 9.4
Orion KL	22 GHz (H_2O)	1.9; 3.4
W75N	1.665 & 1.667 GHz (OH)	0.1–0.3; 0.1–0.8
Onsala 1	1.665 GHz (OH)	0.2–0.7; 1.0–1.9
W3(OH)	22 GHz (H_2O)	3.9
NGC4258	22 GHz (H_2O)	1.3

call for proposals are published at the RadioAstron project website [2]. The main objectives of this phase of the maser program are studying the kinematics and dynamics of the compact sources of maser emission in star-forming regions, as well as the study of extragalactic masers, such as NGC3079 and NGC4258. As a result, along with star-forming regions the signal from extragalactic maser NGC4258 was detected. This maser is associated with the accretion disk around super-massive black hole at the center of this galaxy. The projected baseline in this observing session was up to 2 ED, which corresponds to an angular resolution of 110 μas.

2.2 General statistics of maser source detections

This section provides statistics from the beginning of RA maser observations (November 2011) up to the present time (July 2015). During four years of operation a large amount of data was accumulated, and this allows us to sum up the first results of this work. 135 maser observation sessions were conducted, and 31 sources were observed. The majority of masers observed in RA program are related to star-forming regions – 19 sources in total. Eight masers sources in the envelopes of late-type stars of the Galaxy were observed, and 4 extragalactic masers in star-forming regions and circum-nuclear disks of external galaxies were observed.

Due to technical reasons the scientific data have been corrupted or lost in 10 sessions out of total 135. 103 observations of the remaining 125 sessions at the moment (August 2015) are processed, positive detections are obtained in 21 sessions. Thus, the current detection rate of fringes at space-ground baselines is about 20.4 %. Some scientific data is still under consideration at ASC LPI data processing center [3]. The final detection rate is likely to be higher.

All successful fringe detections for galactic masers at space-ground baselines were obtained for the sources associated with star-forming regions, – 20 positive detections. One detection was obtained for extragalactic maser. No fringes for the stellar masers were obtained at space-ground baselines yet. Probably, the spots of the brightest masers in the stellar envelopes are fully resolved at the space-ground baselines.

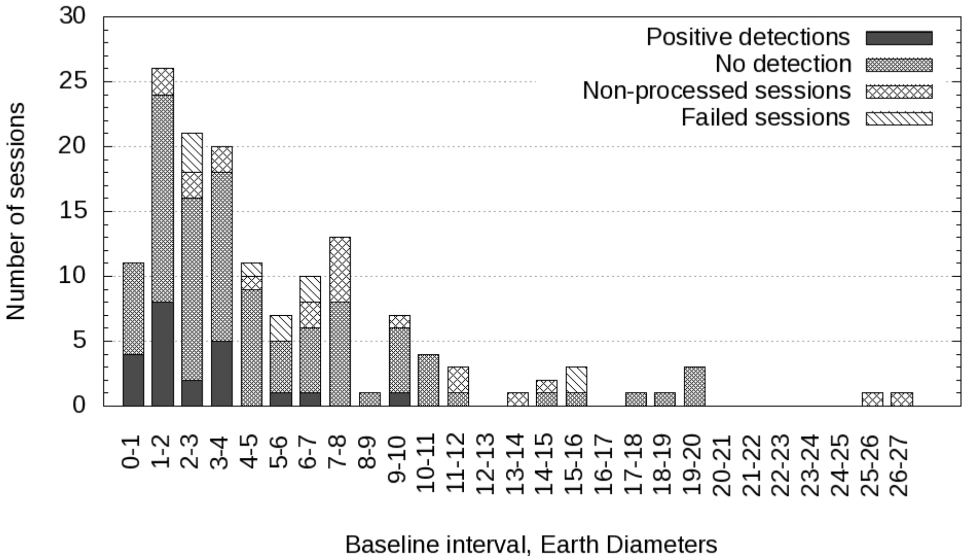

Figure 1: Statistics of maser observation results over projected baseline length of the space interferometer RadioAstron.

Table 1 provides information on the observational sessions which provided positive fringe detection with the space interferometer. The columns show source names, observed lines and projected lengths of the space-ground baselines at which the interferometric detection was obtained. Each baseline (or baseline interval) corresponds to one observational session with positive detection of the fringes.

It is instructive to show the distribution of the number of detections depending on the length of the baseline projection. Figure 1 presents statistics of observational sessions for the whole set of database lengths. It is seen that most of the positive detections fall in range from 1 to 4 ED.

3 Estimates of the minimal brightness temperatures for the maser sources of the Galaxy

Brightness temperature is one of the observational parameters of the maser emission which provides a basic and strong constraint on the theoretical models of maser pumping. Usually the brightness temperature is estimated from the source imaging using adequate range of baseline projections. This way requires involvement of many telescopes and a rather long duration of observations in order to obtain good sampling of the uv-plane. But at present the majority of RadioAstron maser data consists of the short observations with duration of about 1 hour with a few baseline sets, about 3 to 6. These are detection experiments which do not allow producing map of the source. Nevertheless, using some assumptions it is possible to estimate brightness temperature and size of the source even for such short sessions.

Table 2: Brightness temperature estimates for some H_2O masers observed by RadioAstron

Source	Baseline, ED	Resolution, μas	Minimal T_b, K	T_b, K
W3 IRS5	3.5	62	9.0×10^{14}	1.5×10^{15}
W3 IRS5	5.4	40	1.5×10^{15}	8×10^{15}
W3 OH	3.8	58	2.1×10^{14}	7×10^{14}
Cepheus A	3.4	64	1.2×10^{14}	3×10^{14}
Orion	3.3	66	1.2×10^{15}	6×10^{15}
W49N	9.6	23	4.5×10^{14}	2.6×10^{15}

For example, we can assume that the shape of the brightness distribution is a circular Gaussian. This proved to be a good approximation in many observed cases. Under this assumption we can estimate brightness temperature of the source using the formula proposed in [5]

$$T_\mathrm{b} = \frac{\pi}{2k} \frac{B^2 V_0}{\ln\left(V_0/V_q\right)}. \qquad (1)$$

Here B is a baseline, V_q is an amplitude of visibility function at a single spatial frequency $q = B/l$, and V_0 is a space-zero visibility. It was shown [5] that T_b has its lowest value when $V_0/V_q = e$. This provides the minimal brightness temperature estimate $T_\mathrm{b,min}$ when the values of baseline and correlated flux are obtained from observations

$$T_\mathrm{b,min} \approx 3.09 \left(\frac{B}{\mathrm{km}}\right)^2 \left(\frac{V_q}{\mathrm{mJy}}\right) [K]. \qquad (2)$$

Principles of the maser data processing have basic similarities to continuum data processing. However, maser observations greatly depend on the proper selection of the frequency band and need a large number of frequency channels for correlation. This imposes additional requirements on the correlator software. We carried out post-correlation data processing using the VLBI processing software package PIMA [4]. Source fluxes were calibrated using system temperature measurements provided by the telescopes participating in observations with RA.

4 Results and conclusions

Here we discuss some estimates of T_b and $T_\mathrm{b,min}$ obtained from the measured source flux S under the assumption that the brightness distribution is a circular Gaussian. Some results for compact features detected in star-forming regions W3 IRS5, Orion KL, W3 and Cepheus A are presented in Table 2. Each line corresponds to one observational session. In the second column the baselines in units of ED's are given. In the third column resolution in micro-arcseconds is given. The last two columns show estimates of the brightness temperatures T_b and $T_\mathrm{b,min}$ in Kelvin. The highest temperature is obtained for W3 IRS5 source (8×10^{15} K). Angular resolution is very high, so we observe very compact features of about 20 to 60 micro-arcseconds. Such angular sizes correspond to linear sizes of about 5–10 million km or several solar diameters.

The main conclusions of the work are the following:

1. Space-VLBI observations of the water and hydroxyl masers show that the bright details of the masers in galactic star-forming regions often remain unresolved at baseline projections which considerably exceed Earth diameter. Record resolution for the maser observations at present are obtained for W49N water maser – 23 micro-arcsec at projected baseline 9.6 ED.
2. Very compact water maser features with the angular sizes of about 20–60 micro-arcseconds are registered in galactic star-forming regions. These correspond to linear sizes of about 5–10 million km (several solar diameters).
3. Estimates of the brightness temperatures for the ultracompact interstellar water maser features range from $\sim 10^{14}$ to $\sim 10^{16}$ K.

Acknowledgments. The RadioAstron project is led by the Astro Space Center of the Lebedev Physical Institute of RAS and the Lavochkin Association of Russian Federal Space Agency, and is a collaboration with partner institutions in Russia and other countries. This research is partly based on observations with the 100 m telescope of the MPIfR at Effelsberg; radio telescopes of IAA RAS (Federal State Budget Scientific Organization Institute of Applied Astronomy of Russian Academy of Sciences); Medicina & Noto telescopes operated by INAF – Istituto di Radioastronomia; Hartebeesthoek, Torun, WSRT, Yebes, and Robledo radio observatories. The National Radio Astronomy Observatory is a facility of the National Science Foundation operated under cooperative agreement by Associated Universities, Inc. Results of optical positioning measurements of the Spektr-R spacecraft by the global MASTER Robotic Net [6], ISON collaboration, and Kourovka observatory were used for spacecraft orbit determination in addition to mission facilities.

References

1. *N.S. Kardashev, A.V. Alakoz, Y.Y. Kovalev et al.*, Solar Syst. Res., **49**, 573, 2015.
2. *RadioAstron – Space VLBI Mission*, *http://www.asc.rssi.ru/radioastron*
3. *N.S. Kardashev, V.V. Khartov, V.V. Abramov et al.*, Astron. Rep., **57**, 153, 2013
4. *L. Petrov*, PIMA – VLBI processing software, 2015, *http://astrogeo.org/pima*
5. *A. Lobanov*, Astron. Astrophys., **574**, A84, 2015.
6. *V. Lipunov, V. Kornilov, E. Gorbovskoy et al.*, Adv. Astron., **2010**, 349171, 2010.

Metal Ions in the Circumgalactic Medium

E.O. Vasiliev[1,2], M.V. Ryabova[1], Yu.A. Shchekinov[3]

E-mail: *eugstar@mail.ru*

Recent observations show high column densities of metal ions in extended haloes of galaxies within $z \sim 0$–0.5. For instance, to explain column densities of OVI ion observed around star-forming galaxies one should assume solar metallicity in the extended haloes, and in this case the haloes become the main reservoir of missing baryons and metals. Using time-dependent radiation field of a nearby starburst galaxy we study how ionic species depend on the galactic mass and star formation rate. We derive conditions for the high ionic states of metals to appear in extended galactic haloes.

1 Introduction and model description

High column densities of OVI and CIV ions in halos of star-forming galaxies lead to a conclusion on more massive galactic halos than thought before [1, 2]. In principle, this conclusion for galactic haloes to bear such a large gas mass might solve the problem of missing baryons and metals, though requiring enormously high oxygen production and mass ejection rates. Taking into account galactic ionizing radiation, the maximum OVI fraction can reach ~0.4–0.9 that facilitates constrains on both gaseous mass and metallicity for massive star-forming galaxies [3]. Here we are interested in metal column densities in circumgalactic medium of less massive galaxies with special attention for CIV and OVI ions. We present only a brief description of our model, the details will be presented in our future paper.

Using the photoionization code CLOUDY [4] we calculate all ionization states of the elements H, He, C, N, O, Ne, Mg, Si and Fe. In our calculations the gas in the circumgalactic medium is in local thermal equilibrium that means the equality between cooling and heating rates in a gas parcel located at the radial distance r from the galactic center and exposed to both galactic (reached to such distance) and extragalactic radiation. In order to follow evolution of stellar mass, metallicity and galaxy spectrum, we use the spectrophotometric code PEGASE [5]. We assume a Schmidt-like power-law star formation rate (SFR) typical of star-forming galaxies: $\mathrm{SFR}(t) = \mathcal{M}_g^{p_1}/p_2$, where $\mathcal{M}$ is the normalized mass of gas in $M_\odot$. In our model we assume a closed-box regime. To extend the spectrum to higher energies (up to $\sim 10^4$ eV), we use the empirical relation between the X-ray luminosity and the star formation rate [6]. For the extragalactic background we accept the

[1] Southern Federal University, Russia
[2] Special Astrophysical Observatory, Russian Academy of Sciences (RAS), Russia
[3] Astro Space Center of Lebedev Physical Institute of RAS, Russia

V. Grinin et al. (eds) Radiation mechanisms of astrophysical objects. Yerevan: Edit Print, 2017, pp. 127–132.

Table 1: List of the main models

Total mass of gas $M_g^i, M_\odot$	p_2, Myr/$M_\odot$ (Name of model)		
10^{10}	3×10^5 (A1),	3×10^4 (A2),	3×10^3 (A3)
5×10^{10}	3×10^5 (B1),	3×10^4 (B2),	3×10^3 (B3)
10^{11}	3×10^5 (C1),	3×10^4 (C2),	3×10^3 (C3)

spectrum described in [7]. We suppose the density profile has a shape similar to the Milky Way galaxy [8] normalized to mass of the dark matter halo. The parameters of the models are listed in Table 1. A fiducial value of gas metallicity in our models is assumed to be equal to 0.1 $Z_\odot$.

2 Results

We consider gas in outer haloes of star-forming galaxies with stellar mass $\sim 10^9 - 10^{11}$ $M_\odot$. Figure 1 shows the dependence of specific star formation rate, sSFR = SFR/M_*, on the stellar mass, M_*. Note that the value of p_2 increases from left to right. It is clearly seen that almost all points for the COS-Dwarfs galaxies are locked between tracks for models A1–C2 as well as the data for the star-forming COS-Halos galaxies are close to the tracks of the models C2–C3. Therefore, we expect that spectral properties of the galaxies observed in the COS-Dwarfs and COS-Halos surveys are similar to those in the models considered here during the latest ~3–4 Gyrs of their evolution.

Figure 2 shows the dependence of CIV column densities (left panels) in a halo around a galaxy in models B*. The N(CIV) values become lower with a decrease of both impact distance b and HI column density in the disk. This is explained by an increase of photons ionized CIV, so that under such conditions carbon is locked mainly in CV state. High column densities, $N(\mathrm{CIV}) \gtrsim 10^{14}$ cm^{-2}, are found at impact distances $b \lesssim 0.3\, r_v$, moderate values $\sim 10^{13.5}$–10^{14} cm^{-2} can be detected at larger distances $b \sim (0.3$–$0.5)\, r_v$. Certainly, the increase of SFR from model B1 (upper panel) to B3 (lower panel) leads to reducing N(CIV), especially this is clear for moderate values of HI column density $\sim 10^{20}$–$10^{20.4}$ cm^{-2}. However, the N(CIV) values calculated for galaxies in models B* and $N(\mathrm{HI}) \gtrsim 10^{20.4}$ cm^{-2} are close to the measured ones in the COS-Dwarfs survey [2]. Note that the stellar masses and SFR in models B* are also similar to those detected for the host galaxies in the survey (Fig. 1). One can see that N(CIV) significantly depends on the absorption of galactic radiation.

Figure 2 shows the OVI column densities (right panels) in a halo around a galaxy in models B*. Similar to N(CIV) the OVI column density reaches values as high as $\sim 10^{13.8}$ cm^{-2} at $b \lesssim 0.5\, r_v$, but contrary to CIV it increases for smaller absorption of the galactic radiation: N(OVI) becomes $\sim 10^{14.2-15}$ cm^{-2} for $N(\mathrm{HI}) \lesssim 10^{20.3}$ cm^{-2}. Higher SFR is also favor to higher N(OVI). Such behavior is due to a growth of galactic photons being able to ionize OV.

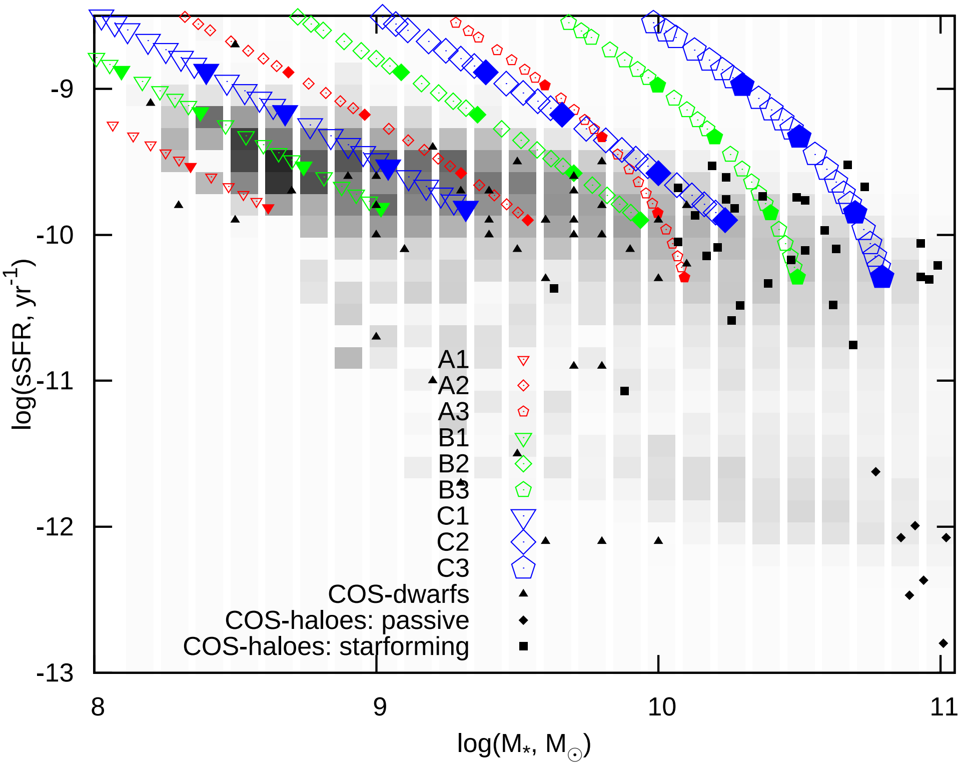

Figure 1: The dependence of specific star formation rate, sSFR $=$ SFR$/M_*$, on the stellar mass, M_*, for the models A*, B* and C* showed by small, middle-size and large open symbols (Table 1). The value of p_2 increases from left to right. The filled symbols among open ones correspond to 1, 2, 5 and 10 billion years (from top-left to bottom-right points) passed from the beginning of the evolution of a galaxy. Data for the COS-Dwarfs galaxies from [2] are shown by small filled triangles and for the COS-Halos star-forming and passive galaxies from [1] are depicted by small filled squares and rhombuses, respectively. The gray-scale map is for SDSS+GALEX galaxies [9].

Note that both CIV and OVI column densities are as high as $\sim 10^{14-14.5}$ cm^{-2} and $\sim 10^{14.5-15}$ cm^{-2}, respectively, at small $b \lesssim 0.2$ for moderate values of $N(\mathrm{HI}) \sim 10^{20.4}$ cm^{-2}. Whereas in other ranges of $N(\mathrm{HI})$ and b either CIV or OVI has high column density, in other words, there takes place the bimodal distribution. It has been argued [2] that high CIV column densities can be found in halos of dwarf galaxies, whereas high OVI values are usual in a gas around massive star-forming galaxies [1], and have assumed the existence of bimodality over mass of a galaxy. Here we consider the same total and initial gaseous masses of a galaxy (in models B* the initial gaseous mass equals 5×10^5 $M_\odot$, see Table 1), but the SFR is taken different, so that during the evolution the stellar masses reach different values ranged by more than an order of magnitude (middle-size green symbols in Fig. 1). However, Figure 2 shows similar $N(\mathrm{OVI})$ distributions for all three values of SFR and significant dependence of $N(\mathrm{OVI})$ on HI column density.

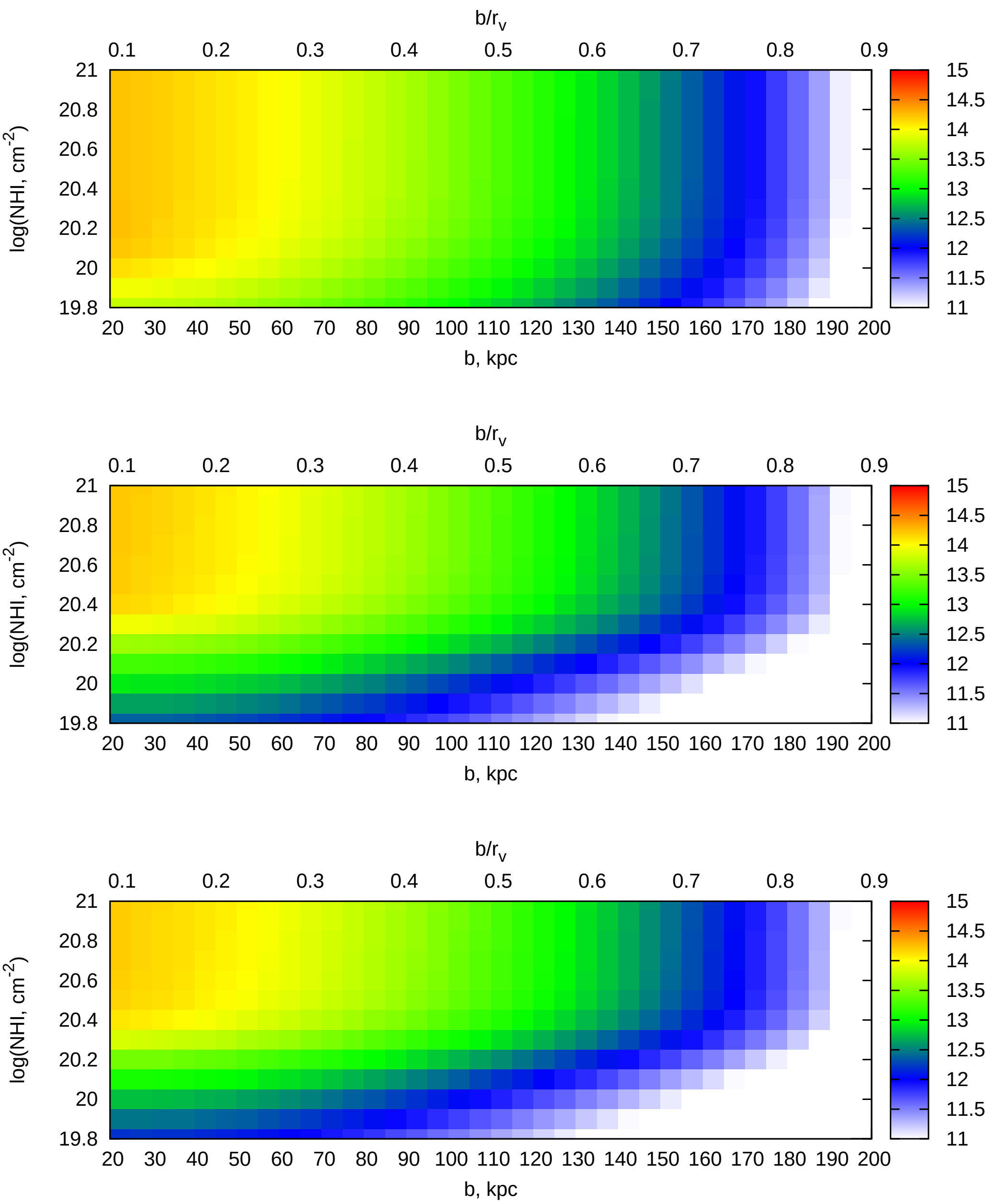

Figure 2: The dependence of CIV (*left* panels) and OVI (*right* panels) column densities (in logarithmic scale) in a halo around a galaxy in models B* on impact parameter b (which is given in kpc in the lower x-axis and in units of virial radius r_v of a galaxy in the upper x-axis) and the HI column density $\log N_{\rm HI}$ in the galactic disk. The upper row corresponds to model B1 ($M = 5\times10^{10}\ M_\odot$, $p_2 = 3\times10^5$ Myr/$M_\odot$), the middle is for model B2 ($M = 5\times10^{10}\ M_\odot$, $p_2 = 3\times10^4$ Myr/$M_\odot$), and the lower one is for B3 ($M = 5\times10^{10}\ M_\odot$, $p_2 = 3\times10^3$ Myr/$M_\odot$). The virial radius r_v of a galaxy with $M = 5\times10^{10}\ M_\odot$ at $z = 0$ equals $\sim$218 kpc.

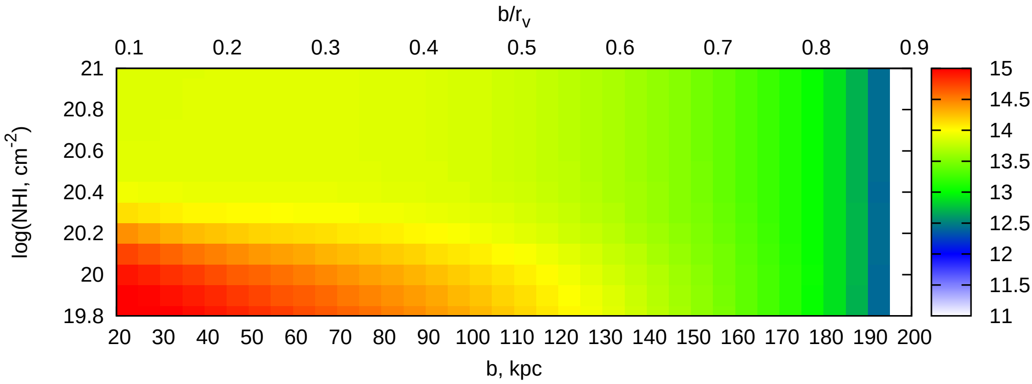
b/r_v
0.1 0.2 0.3 0.4 0.5 0.6 0.7 0.8 0.9
log(NHI, cm^-2)
21 20.8 20.6 20.4 20.2 20 19.8
15 14.5 14 13.5 13 12.5 12 11.5 11
20 30 40 50 60 70 80 90 100 110 120 130 140 150 160 170 180 190 200
b, kpc

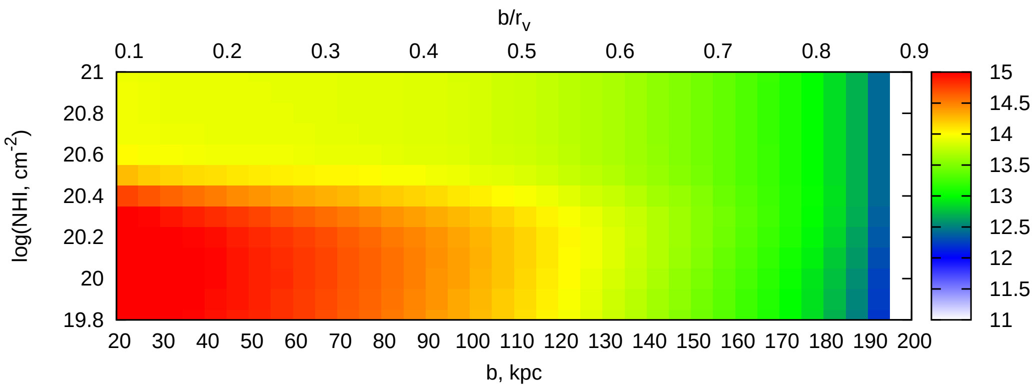
b/r_v
0.1 0.2 0.3 0.4 0.5 0.6 0.7 0.8 0.9
log(NHI, cm^-2)
21 20.8 20.6 20.4 20.2 20 19.8
15 14.5 14 13.5 13 12.5 12 11.5 11
20 30 40 50 60 70 80 90 100 110 120 130 140 150 160 170 180 190 200
b, kpc

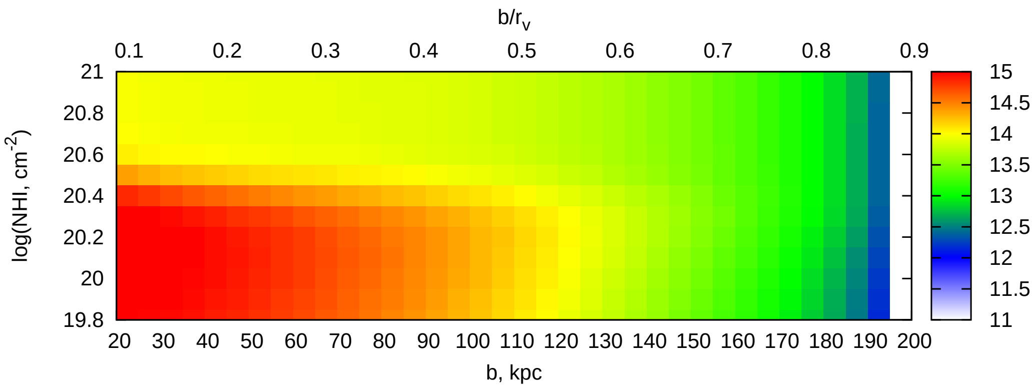
b/r_v
0.1 0.2 0.3 0.4 0.5 0.6 0.7 0.8 0.9
log(NHI, cm^-2)
21 20.8 20.6 20.4 20.2 20 19.8
15 14.5 14 13.5 13 12.5 12 11.5 11
20 30 40 50 60 70 80 90 100 110 120 130 140 150 160 170 180 190 200
b, kpc

Acknowledgments. E.V. is supported by the Russian Scientific Foundation (grant 14-50-00043). M.R. and Y.S. are supported by the RFBR (grants 15-02-08293, 15-52-45114).

References

1. *J. Tumlinson, C. Thom, J.K. Werk et al.*, Science, **334**, 948, 2011.
2. *R. Bordoloi, J. Tumlinson, J.K. Werk et al.*, Astrophys. J., **796**, 136, 2014.
3. *E.O. Vasiliev, M.V. Ryabova, Yu.A. Shchekinov*, Mon. Not. Roy. Astron. Soc., **446**, 3078, 2015.
4. *G.J. Ferland, K.T. Korista, D.A. Verner et al.*, Publ. Astron. Soc. Pacif., **110**, 761, 1998.
5. *M. Fioc, B. Rocca-Volmerange*, Astron. Astrophys., **326**, 950, 1997.
6. *M. Gilfanov, H.-J. Grimm, R. Sunyaev*, Mon. Not. Roy. Astron. Soc., **347**, L57, 2004.
7. *F. Haardt, P. Madau*, in Clusters of Galaxies and High Redshift Universe Observed in X-rays. Eds. D.M. Neumann, J.T.V. Tran. Rencon. Moriond, 2001.
8. *R. Feldmann, D. Hooper, N.Y. Gnedin*, Astrophys. J., **763**, 21, 2013.
9. *D. Schiminovich, T.K. Wyder, D.C. Martin et. al.*, Astrophys. J. Suppl., **173**, 315, 2007.

* The color figures are available online in the Proceedings at *http://www.astro.spbu.ru/sobolev100/*.

Energy Budget in Multiple Supernova Explosions

E.O. Vasiliev[1,2], B.B. Nath[3], Yu.A. Shchekinov[4]

E-mail: *eugstar@mail.ru*

Standard models of large scale galactic outflows in starburst galaxies assume a high efficiency of SNe in heating the gas in central regions of starburst galaxy in order to launch outflows. We study the heating efficiency of the interstellar gas by multiple supernovae (SNe) within 3D simulations. We argue that SNe remnants have to act coherently in space and in time in order to minimize radiative losses. We show that interacting expanding shells from different SNe restrict the heating efficiency of multiple SNe even when they explode with a high rate. As a result the heating efficiency can considerably differ from a commonly assumed value (0.1–0.3).

1 Introduction

Heating of the interstellar medium by multiple supernovae (SNe) explosions is at the heart of producing galaxy-scale outflows in starburst galaxies. Standard models of outflows assume a high efficiency of SNe in heating the gas to X-ray emitting temperatures and filling the central region of starburst with hot gas, in order to launch vigorous outflows. The collective effect of clustered SNe is believed to form a superbubble (e.g., [1]) whose shell of swept up mass moves faster than the typical speed of OB associations (few km s^{-1}) and which therefore contains most of the SNe arising from the association. The study of the evolution of these superbubbles has mostly assumed continuous energy release from the center.

This problem becomes acute in the context of supernovae driven galactic winds in which it is assumed that SNe can sufficiently heat up the ISM gas, at least in the central region of disc galaxies, in order to launch a wind. This process assumes that although SNe lose most energy in radiation in isolated cases, the efficiency of heating the ISM can be large in the central region filled with hot and low density gas and that the gas in this region is thermalized [2, 3]. Numerical simulations (e.g., [4, 5, 6]) also implement the initial conditions leading to galactic winds making similar assumptions. It is believed that in a multiphase medium and in the case of multiple SNe events, the efficiency of SNe heating – the fraction of the total explosion energy transferred into thermal energy – can be larger than $\sim$0.1. These

[1] Southern Federal University, Russia
[2] Special Astrophysical Observatory, Russian Academy of Sciences (RAS), Russia
[3] Raman Research Institute, India
[4] Astro Space Center of Lebedev Physical Institute of RAS, Russia

V. Grinin et al. (eds) Radiation mechanisms of astrophysical objects. Yerevan: Edit Print, 2017, pp. 133–136.

estimates came from the numerical and analytical studies of energy loss in *isolated* supernova remnants, which showed that the fractional energy retained in the hot interior gas of remnants was of order $\sim$0.1. Larson [7] had first pointed out the importance of cooling with regard to galactic outflows, and derived a critical supernova rate density required to compensate for cooling.

The question of heating efficiency of SNe crucially depends on the evolution of multiple SNe which has not yet been studied in detail. Nath and Shchekinov [8] have argued that the energy input from multiple SNe in the central regions of starbursts cannot heat the gas to $T \geq 10^6$ K unless the SNe events act coherently in space and time. Here we study two aspects of the problem of multiple SNe with gas-dynamic simulations, namely, we test the importance of coherency condition and consider the time scale and conditions under which percolation of hot gas becomes possible. This allows us to study the efficiency of heating by multiple SNe events, in particular the efficiency of heating gas to high temperature.

2 Numerical method and initial conditions

We use three-dimensional unsplit TVD code based on the MUSCL-Hancock scheme and the HLLC method (e.g., [9]) as an approximate Riemann solver. In the energy equation we take into account cooling processes adopted the tabulated non-equilibrium cooling curve [10]. This cooling rate is obtained for a gas cooled isobarically from 10^8 down to 10 K. The heating rate is adopted to be constant whose value is chosen so that the background gas does not cool.

We have carried out 3-D gasdynamic simulations (Cartesian geometry) of multiple SNe explosions using periodic boundary conditions. The computational domains have size 200^3 pc^3 which consists of 300^3 cells corresponding to a physical cell size of 0.75 pc. The background number density considered ranges between 0.1–10 cm^{-3}, the background temperature is 10^4 K. The metallicity is constant within the domain, and we consider the cases with $Z = 0.1$, 1 $Z_\odot$. We inject the energy of each SN in the form of thermal energy in a region of radius $r_i = 1.5$ pc. SNe are distributed uniformly and randomly over the computational domain.

3 Results

We have performed runs with SNe exploding continuously in the computational domain of 200^3 pc^3 with resolution of 1 pc and gaps of $\Delta t = 10^3$, 10^4, 2×10^4, 3×10^4, 4×10^4 and 10^5 yr. In other words, one supernova explodes after every Δt. The positions of SNe are distributed randomly in space. Figure 1 shows the results of heating efficiencies (left) and filling factors (right) for gas with different temperatures, for all time delays (from short to long delays, from top to bottom). We denote the efficiency of heating gas to $\geq 10^{6.5}$ K by $\eta[10^{6.5}]$ and define it as the ratio of thermal energy stored in gas with $T \geq 10^{6.5}$ K at any given time to the total explosion energy deposited up to that time. It is clear that the case of more frequent SNe ($\Delta t = 10^3$ yr) shows continuous decline in the

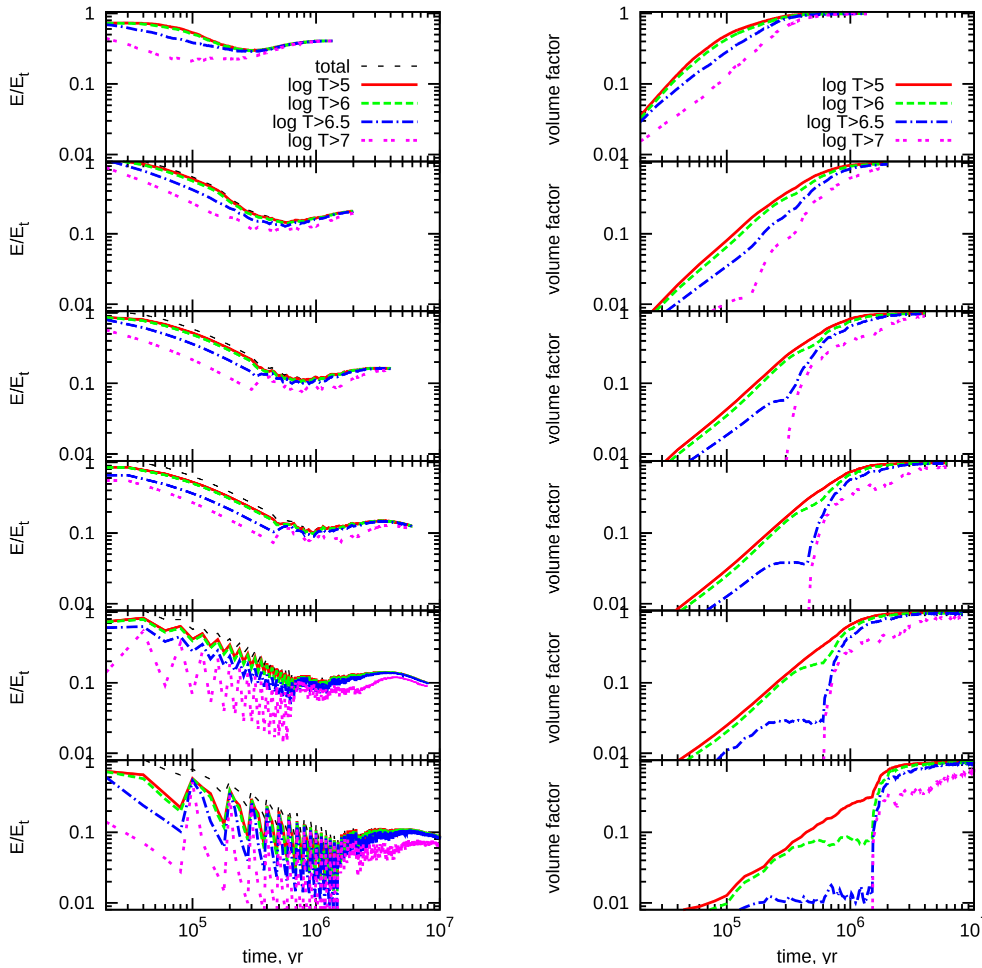

Figure 1: The evolution of the heating efficiency (left) and filling factors (right) for gas with different temperatures for a continuous series of SNe separated by time delay $\Delta = 10^3$, 10^4, 2×10^4, 3×10^4, 4×10^4, 10^5 yr (from top to bottom).

heating efficiency $\eta[10^{6.5}]$ and only after $t \simeq 10^5$ yr when the remnants practically fill the whole computational domain (60% of the volume), η increases to $\sim$0.4 because the subsequent SNe mostly expand into hot diffuse medium. Explosions with a longer delay of $\Delta t = 10^5$ yr (bottom most row) show on average similar trend on longer time scales, though as expected, with lower heating efficiency of order $\eta[10^{6.5}] \sim 0.1$. Similar to the previous model, the efficiency first declines and then increases after the remnants occupy roughly 30% of the computational zone at $t \simeq 10^6$ yr to $\eta[10^{6.5}] \sim 0.1$.

A common feature in the behavior of the heating efficiency in all models can be obviously noted: after a continuous decline down to $\eta(T) \lesssim 0.1$, it stabilizes and then grows slowly for all temperature fractions, particularly for the gas with $T \geq 3\times10^6$ K which carries a considerable amount of thermal energy. The most reasonable explanation is that the epoch of increasing η coincides with the state when the filling factor of the corresponding temperature fraction reaches a critical value $f(T) \sim 0.3$ when different bubbles percolate.

The time required for the percolation of hot gas can be found by using the result that the threshold filling factor is ∼0.3 and can be estimated as [11]

$$t_{\rm perc} \approx 10\,{\rm Myr} \left(\frac{n}{E_{51}}\right)^{4/7} \left(\frac{\nu_{\rm SN}}{10^{-10}\,{\rm pc}^{-3}\,{\rm yr}^{-1}}\right)^{-4/7}. \quad (1)$$

For a typical starburst SNe rate density of $\sim 10^{-9}$ pc^{-3} yr^{-1} and gas density of $n \sim 10$ cm^{-3} in starburst nuclei, the time scale for heating efficiency to become ≥ 0.1 is of order 10 Myr.

It is interesting to note that recent observations of 10 starburst galaxies show that there is a time lag of ∼10 Myr between the onset of star formation and the excitation of galactic winds [12]. Our simulations and the important result of percolation of hot gas when the overall filling factor crosses a threshold of ∼0.3, therefore, allow us to interpret this time lag as required for heating efficiency to become sufficiently large for an outflow to be launched.

Using our simulations for different gas densities (n = 0.3, 1, 3, 10 cm^{-3}) and keeping the SNe frequency a constant, we can infer the scaling of the heating efficiency with the SNe rate density and ambient density [11]. We find that roughly $\eta[10^{6.5}] \propto \nu_{\rm SN}^{0.2}\, n^{-0.6}$ for the heating efficiency of X-ray emitting gas.

Acknowledgments. E.V. is supported by the Russian Scientific Foundation (grant 14-50-00043). Yu.S. is grateful for partial support from the RFBR through the grants 15-02-08293 and 15-52-45114.

References

1. *M-M. Mac Low, R. McCray*, Astrophys. J., **324**, 776, 1988.
2. *R.A. Chevalier, A.W. Clegg*, Nature, **317**, 44, 1985.
3. *M. Sharma, B.B. Nath*, Astrophys. J., **763**, 17, 2013.
4. *A.A. Suchkov, D.S. Balsara, T.M. Heckman, C. Leitherer*, Astrophys. J., **430**, 511, 1994.
5. *D. Strickland, I.R. Stevens*, Mon. Not. Roy. Astron. Soc., **314**, 511, 2000.
6. *A. Fujita, C.S. Marttin, M.-M. Mac Low et al.*, Astrophys. J., **698**, 693, 2009.
7. *R. Larson*, Mon. Not. Roy. Astron. Soc., **169**, 229, 1974.
8. *B.B. Nath, Yu.A. Shchekinov*, Astrophys. J. Lett., **777**, L12, 2013.
9. *E. Toro*, Riemann Solvers and Numerical Methods for Fluid Dynamics. A Practical Introduction. Berlin: Springer-Verlag, 1999.
10. *E.O. Vasiliev*, Mon. Not. Roy. Astron. Soc., **431**, 638, 2013.
11. *E.O. Vasiliev, B.B. Nath, Yu.A. Shchekinov*, Mon. Not. Roy. Astron. Soc., **446**, 1703, 2015.
12. *R.G. Sharp, J. Bland-Hawthorn*, Astrophys. J., **711**, 818, 2010.

* The color figure is available online in the Proceedings at *http://www.astro.spbu.ru/sobolev100/*.

Dust in Outer Layers of B5 Globule

V.B. Il'in[1,2], Y.S. Efimov[3], T.N. Khudyakova[1], M.S. Prokopjeva[1]

E-mail: *ilin55@yandex.ru*

We present results of $UBVRI$ polarimetry of about 30 stars in a vicinity of the well-studied Bok globule Barnard 5 (B5). We find a correlation of the maximum polarization wavelength λ_{max} with extinction in the cloud when $A_V > 1.5$ mag. We conclude that multicolor polarimetry of background stars can be a useful tool to characterize dust in outer regions of dark clouds.

The properties of dust in dark clouds are still not well understood. Recent studies of extinction law, scattered light and submm emissivity have inferred changes in dust properties with an increase of depth inside a cloud (e.g., [1]). However, there are doubts that the wavelength dependence of polarization $P(\lambda)$ of background stars can be useful to characterize dust grains as different factors can affect this dependence in typical molecular clouds [2]. For globules, being smaller and more simple geometrically and physically, the situation can be different, but observations of $P(\lambda)$ variations with the depth have not been made since the work [3].

We performed $UBVRI$ polarimetric observations of about 30 stars around B5 at 2.6-m ZTS and 1.25-m AZT-11 telescopes with the standard equipment at the Crimea Observatory in 1990–93. These polarimetric data supplemented with those available in the literature allowed us to derive much more reliable estimates of λ_{max} than in [3] (see as examples the values of λ_{max} in micron in the table).

Stars	data from [3]	this work
J1	0.79 ± 0.06	0.77 ± 0.02
J6	0.80 ± 0.11	0.55 ± 0.06

Stars	data from [3]	this work
J2	0.85 ± 0.08	0.76 ± 0.02
J16	1.11 ± 0.29	0.93 ± 0.12

For 20 out of 36 stars considered, we accepted the spectral classes found from Vilnius system photometry in [4]. For other 8 stars, we took the classes given by HDEC and assumed that the stars belong to the MS. For the weakest rest 8 stars, we estimated spectral classes from 2MASS data in a usual way. That gave us estimates of A_V and distances to the stars as photometric data are available.

We used data from the COMPLETE survey that has given various detailed maps of several star-forming regions including that in Perseus with the globule B5 being located at its edge [5]. In the figure we show a map of B5 with the

[1] Sobolev Astronomical Institute of St.Petersburg University, Russia
[2] Pulkovo Observatory of the RAS, Russia
[3] Crimea Astrophysical Observatory, Crimea

V. Grinin et al. (eds) Radiation mechanisms of astrophysical objects. Yerevan: Edit Print, 2017, pp. 137–138.

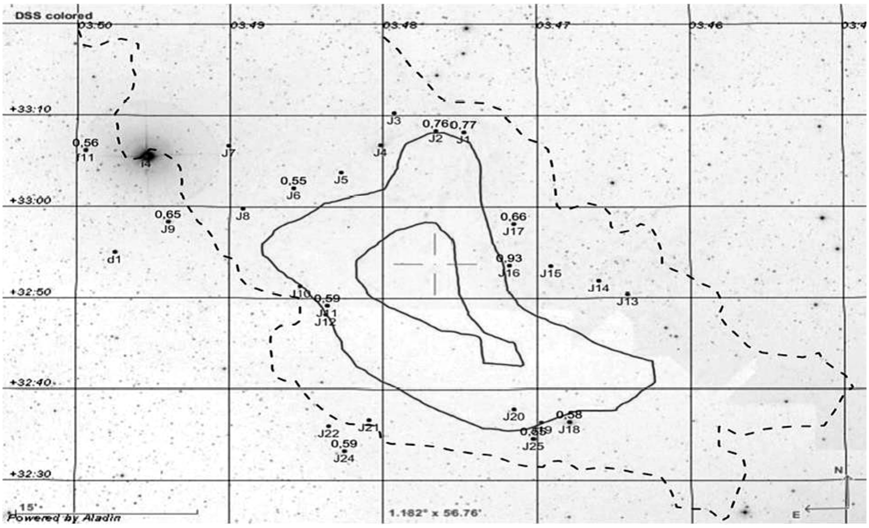

Figure 1: Map of B5 globule. Continuous lines present the extinction contours with $A_V = 3$ and 5 mag from [5]. Points with the number marks show our stars. Numbers above these marks give the obtained values of λ_{max} in micron.

extinction contours from this survey (and our stars with λ_{max} values derived). We find a good agreement of our estimates of A_V with those of [5].

For the field stars, we found locally increased $\lambda_{max} \approx 0.6 \pm 0.05\,\mu$m, which is typical of star-forming regions and is usually related to an effect of close stars.

Our data show that the stars J11, J18, J25 and F11 are foreground as the distance to them is less than that to B5 (~350 pc). For other stars, we see a certain increase of λ_{max} values when the cloud contribution to A_V grows.

Generally, we did not find clear effects of the halo on the maximum polarization wavelength, but detected a certain increase of λ_{max} when the contribution of the outer layers was significant ($A_V > 1.5$ mag).

Acknowledgments. The work was supported by grants RFBR 16-02-00194 and DST-RFBR 16-52-45002.

References

1. *J.B. Foster, K.S. Mandel, J.E. Pineda et al.*, Mon. Not. Roy. Astron. Soc., **428**, 1606, 2013.

2. *B.G. Andersson, A. Lazarian, J.E. Vaillancourt*, Ann. Rev. Astron. Astrophys., **53**, 501, 2015.

3. *H.C. Bhatt*, Mon. Not. Roy. Astron. Soc., **222**, 383, 1986.

4. *K. Cernis*, Balt. Astron., **2**, 214, 1993.

5. *N.A. Ridge, J. Di Francesco, H. Kirk et al.*, Astron. J., **131**, 2921, 2006.